

# Light curves of oscillating neutron stars

Umin Lee<sup>1</sup>  $\star$  and Tod E. Strohmayer<sup>2</sup>

<sup>1</sup>*Astronomical Institute, Tohoku University, Sendai, Miyagi 980-8578, Japan*

<sup>2</sup>*Laboratory for High Energy Astrophysics, NASA's Goddard Space Flight Center, Greenbelt, MD 20771, USA*

Typeset 18 July 2018; Received / Accepted

## ABSTRACT

We calculate light curves produced by  $r$ -modes with small azimuthal wavenumbers,  $m$ , propagating in the surface fluid ocean of rotating neutron stars. We include relativistic effects due to rapid rotation, and propagate photons from the stellar surface to a distant observer using the Schwarzschild metric. The wave motions of the surface  $r$ -modes are confined to the equatorial region of the star, and the surface pattern of the temperature variation can be either symmetric (for even modes) or anti-symmetric (for odd modes) with respect to the equator. Since for the surface  $r$ -modes the oscillation frequency in the corotating frame of the star is much smaller than the rotation frequency,  $\Omega$ , we employ the approximation in which the oscillation frequency in the inertial frame,  $\sigma$ , is given by  $\sigma = -m\Omega$ . We find that the *even*,  $m = 1$   $r$ -mode produces the largest light variations. The dominant Fourier component in the light curves of these modes is the fundamental having  $\sigma = -\Omega$ , and the first harmonic component having  $\sigma = -2\Omega$  is always negligible in comparison. The dominant Fourier component of the even,  $m = 2$   $r$ -modes is the first harmonic. Although the *odd*  $r$ -modes produce smaller amplitude light variations compared with the *even* modes, the light curves of the former have a stronger first harmonic component. If both  $m = 1$  and  $2$   $r$ -modes are excited simultaneously, a rich variety of light curves is possible, including those having an appreciable first harmonic component. We show that the phase difference,  $\delta - \delta_E$ , between the bolometric light curve and that at a particular photon energy can possibly be used as a probe of the stellar compactness,  $R/M$ , where  $R$  and  $M$  are the radius and mass of the star.

**Key words:** neutron – stars: oscillations – stars : rotation – stars

## 1 INTRODUCTION

It is now widely accepted that millisecond oscillations during thermonuclear X-ray bursts (hereafter, burst oscillations) on accreting, weakly magnetized neutron stars in low mass X-ray binary (LMXB) systems are produced by spin modulation of a slowly moving, non-uniform brightness pattern on the stellar surface (see Strohmayer et al. 1996; Strohmayer & Bildsten 2004, van der Klis 2004). In addition to revealing the spin frequency these oscillations encode information about the global properties of the neutron star. A number of attempts have been made to model burst oscillations and thus to infer these properties (e.g., Nath, Strohmayer & Swank 2001; Muno, Özel & Chakrabarty 2002; Poutanen & Gierliński 2003; Bhattacharyya et al. 2005), however, uncertainties associated with the exact nature of the brightness pattern makes a unique interpretation of the data problematic.

As of February, 2005, the number of LMXBs that exhibit burst oscillations amounts to 13, and two of these contain millisecond X-ray pulsars (see, e.g., Chakrabarty et al. 2003; Strohmayer et al. 2003). For most burst oscillations a single oscillation frequency is found that displays a positive frequency drift  $\Delta\nu_{\text{burst}}$  of a few Hz from the start to the tail of a burst. In the decaying tail the frequency often approaches an asymptotic value (e.g., Strohmayer & Markwardt 1999). The asymptotic frequencies are stable to a few parts in 1000 in bursts observed over several years from any given source (Strohmayer et al. 1998b; Muno et al. 2002a). Background subtracted light curves for the burst oscillations are in most cases well fitted by a

$\star$  E-mail: lee@astr.tohoku.ac.jp; stroh@clarence.gsfc.nasa.gov

single sinusoid, the frequency of which we will call the fundamental frequency. Harmonic content in the light curves is generally small (Strohmayer & Markwardt 1999; Munro et al. 2002b). Indeed, to date there exists only one strong detection of a first harmonic, in the millisecond X-ray pulsar XTE J1814-338 (Strohmayer et al. 2003, Bhattacharyya et al. 2005). On average the rms amplitudes of the burst oscillations are 2%-10%, and generally increase with photon energy (Munro et al. 2003). Munro et al. (2003) also explored the energy dependence of the oscillation phases of burst oscillations. They found either constant phase lags with energy or in some cases evidence for modest hard lags, behavior that is opposite to what one would expect from relativistic motion of a simple hot spot on the stellar surface (e.g., Ford 1999). Interestingly, where phase lags have been measured in the accreting millisecond pulsars they all show soft lags, consistent with a rotating hot spot model (Cui, Morgan & Titarchuk 1998; Poutanen & Gierliński 2003).

As noted above, a non-uniform brightness distribution on the surface of rotating neutron stars is almost certainly responsible for the burst oscillations, and several models have so far been proposed to explain the inhomogeneous pattern. As a typical model, Strohmayer et al. (1997) suggested the oscillation originates from hot regions (hot spots) in a thermonuclear burning layer that expands and decouples from the neutron star at the start of the burst. Although a simple hot spot appears to be consistent with oscillations observed during the onset of some bursts (see Strohmayer et al. 1998a), further calculations suggested that a rigidly rotating, hydrostatically expanding burning layer produces too small a frequency drift (Cumming & Bildsten 2000, Cumming et al. 2002).

There have been numerous efforts to calculate light curves produced by hot spots on the surface of rotating neutron stars (e.g., Pechenick et al. 1983, Chen & Shaham 1989, Strohmayer 1992, Page 1995, Braje et al. 2000, Weinberg et al. 2001, Munro et al. 2002, Nath et al. 2002, Poutanen & Gierliński 2003, Bhattacharyya et al. 2005). In the modeling of the light curves many parameters are employed, for example, the number of hot spots, their location with respect to the rotation axis, their angular sizes, the inclination angle between the line of sight and the rotation axis, the angular dependence of the specific intensity, the temperature of the spots, the temperature contrast between the spots and their surroundings, the mass, radius, and spin frequency of the star. As noted above, burst oscillation light curves are remarkably sinusoidal. Although the light curve amplitudes are dependent on the relativistic parameter  $R/M$ , which is a parameter of particular importance, it is obvious that there remain parameters other than  $R/M$  that affect the amplitudes, such as the angular sizes and locations of the hot spots and the inclination angle (e.g., Pechenick et al. 1983, Weinberg et al. 2001, Munro et al. 2002b). In this sense it is quite important to find other observational quantities that can be used to obtain independent constraints on these parameters. The energy dependencies of phase lags are an example of potentially important observational quantities that carry useful information about the neutron star. Taking account of the special relativistic Doppler boosting of X-ray photons due to rapid rotation of the star (Ford 1999, Weinberg et al. 2001), the hot spot model can produce hard leads more or less consistent with those observed in the millisecond X-ray pulsar SAX J1808.4-3658 and IGR J00291+5934 (Poutanen & Gierliński 2003; Galloway et al. 2005), but the model appears to be at odds with the suggestion of hard lags in some burst oscillations (Munro et al. 2003). Although it may be possible to produce hard lags via a hot Comptonizing corona, it is worth exploring in more detail whether more complex brightness patterns (such as oscillation mode patterns) on the stellar surface might be consistent with the production of hard lags.

By inferring the hot spot size using the observationally obtained blackbody flux  $F_{bb}$ , Poutanen & Gierliński (2003) have succeeded in estimating the radius of the millisecond X-ray pulsar SAX J1808.4-3658 assuming an appropriate range of mass for the star. Recently, Strohmayer et al. (2003) have found the first harmonic component in the light curves of burst oscillations from the accreting millisecond X-ray pulsar XTE J1814-338, and Bhattacharyya et al. (2005) obtained a useful constraint on the ratio  $R/M$  assuming a single hot spot model.

As alluded to above, the hot spot model is not always successful in producing the observed light curves of the burst oscillations. As discussed by Munro et al. (2002b), a small hot spot in a completely dark background is likely to produce light curves with too large an amplitude as well as having strong harmonic components not seen observationally. To suppress the large amplitudes and the harmonics one has to assume, for example, a hot spot of angular size  $\alpha \sim \pi/2$  or almost completely antipodal hot spots, the assumptions of which are not necessarily physically well motivated. It is therefore important to pursue alternatives to the hot spot model.

In this paper, we calculate light curves of rotating neutron stars assuming the surface temperature perturbation pattern caused by surface  $r$ -modes propagating in the fluid ocean of a mass accreting neutron star (Lee 2004). It was Heyl (2004) who first argued that the  $r$ -modes with low  $m$  may play a possible role for burst oscillations. The surface  $r$ -modes are rotationally induced oscillations with very low frequencies in the corotating frame of the star. The  $r$ -modes have dominant vorticity  $(\nabla \times \mathbf{v}')_r$  and are basically just large scale vortexes (see Spitkovsky, Levin, & Ushomirsky 2002). If we assume axisymmetry of the equilibrium configuration of the rotating star, the time dependence of the temperature perturbation may be given by  $e^{i\sigma t}$ , where  $\sigma$  denotes the oscillation frequency in the inertial frame. If we let  $\omega$  and  $\Omega$  denote the oscillation frequency in the corotating frame and the spin frequency of the star, respectively, we have  $\sigma = \omega - m\Omega$ , which leads to  $\sigma \approx -m\Omega$  for the surface  $r$ -modes, since  $|\omega| \ll |m\Omega|$ , where  $m$  is an integer representing the azimuthal wave number around the rotation axis. The time dependence of the perturbation is thus to good approximation given by  $e^{-im\Omega t}$ . Since only the oscillation modes having low  $m$  will produce light variations of appreciable amplitude, in this paper, we only consider the surface  $r$ -modes with

$m = 1$  or  $m = 2$ . We briefly describe the method of calculation in §2. In §3 we discuss some of our numerical results with relevance to burst oscillations. §4 is for a discussion, and we give a summary of our principal conclusions in §5.

## 2 METHOD OF SOLUTION

The method of calculating light curves of rotating neutron stars is similar to those discussed by Pechenick et al. (1983), Page (1995), and Weinberg et al. (2001). Instead of presuming the presence of a hot spot on the surface of a rotating neutron star, we assume that the temperature varies across the surface with the angular distribution appropriate for a surface  $r$ -mode propagating in the fluid ocean of the star. The surface  $r$ -modes, which have very low oscillation frequencies in the corotating frame of the star, can plausibly be excited during thermonuclear bursts (Lee 2004).

To describe oscillations of rotating neutron stars, we employ an  $xyz$  coordinate system whose origin is at the center of the star with the rotation axis along the  $z$  direction. For convenience, we also assume that the observer is in the  $x$ - $z$  plane. In this coordinate system, the oscillations of rotating neutron stars are described by employing spherical polar coordinates  $(r, \theta, \phi)$  with the axis  $\theta = 0$  being the  $z$ -axis. Then, the displacement vector  $\xi(r, \theta, \phi, t)$  is given by

$$\xi_r = \sum_{j=1}^{\infty} S_{l_j} Y_{l_j}^m e^{i\sigma t}, \quad (1)$$

$$\xi_\theta = \sum_{j=1}^{\infty} \left( H_{l_j} \frac{\partial}{\partial \theta} Y_{l_j}^m + T_{l'_j} \frac{1}{\sin \theta} \frac{\partial}{\partial \phi} Y_{l'_j}^m \right) e^{i\sigma t}, \quad (2)$$

$$\xi_\phi = \sum_{j=1}^{\infty} \left( H_{l_j} \frac{1}{\sin \theta} \frac{\partial}{\partial \phi} Y_{l_j}^m - T_{l'_j} \frac{\partial}{\partial \theta} Y_{l'_j}^m \right) e^{i\sigma t}, \quad (3)$$

and the Lagrangian perturbation of the temperature is given by

$$\delta T = \sum_{j=1}^{\infty} \delta T_{l_j} Y_{l_j}^m e^{i\sigma t}, \quad (4)$$

where  $\sigma$  is the oscillation frequency in the inertial frame, and  $Y_l^m$  denotes the spherical harmonic function with degree  $l$  and azimuthal wave number  $m$ , and  $l_j = |m| + 2(j-1)$  and  $l'_j = l_j + 1$  for even modes, and  $l_j = |m| + 2(j-1) + 1$  and  $l'_j = l_j - 1$  for odd modes, and  $j = 1, 2, \dots$ . The functions  $\xi(r, \theta, \phi, t)$  and  $\delta T$  are obtained as a solution to linear differential equations for oscillations of a rotating star, and we need to specify a normalization condition to determine the amplitudes. Since the surface  $r$ -modes have dominant toroidal components  $T_{l'_j}$ , we will employ the amplitude normalization given by  $|\text{Re}[iT_{l'_1}(R)/R]| = 1$ .

The surface temperature of a rotating star that pulsates in various oscillation modes may formally be given by

$$T(R, \theta, \phi, t) = T_0 + \text{Re} \left\{ \sum_{\alpha} C_{\alpha} \left[ \sum_{j \geq 1} \delta T_{l_j}^{\alpha}(R) Y_{l_j}^m(\theta, 0) \right] e^{i(m\phi + \sigma_{\alpha} t)} \right\}, \quad (5)$$

where  $T_0$  is the mean surface temperature,  $\alpha$  indicates a combination of indices that distinguish various oscillation modes, and  $\sigma_{\alpha}$  and  $C_{\alpha}$  denote, respectively, the oscillation frequency and a complex constant representing the amplitudes of the oscillation mode  $\alpha$ . Note that by introducing  $C_{\alpha}$  in equation (5) we mean  $|\text{Re}[iT_{l'_1}^{\alpha}(R)/R]| = |C_{\alpha}|$ . Using the oscillation frequency  $\omega = \sigma + m\Omega$  in the corotating frame, we have

$$m\phi + \sigma_{\alpha} t = m\hat{\phi} + \omega_{\alpha} t, \quad (6)$$

where  $\hat{\phi} = \phi - \Omega t$  is the longitude in the corotating frame.

To consider photon trajectories around a neutron star, it is convenient to introduce another coordinate system  $x'y'z'$ , for which the origin is at the center of the star, and the  $z'$  axis is pointing to the observer and  $y = y'$ . If we let  $i$  denote the inclination angle between the  $z$  axis and the  $z'$  axis, we have

$$x = x' \cos i + z' \sin i, \quad y = y', \quad z = -x' \sin i + z' \cos i, \quad (7)$$

and it is easy to derive the relation between the two spherical polar coordinate systems  $(r, \theta, \phi)$  and  $(r', \theta', \phi')$ , where the axis of  $\theta' = 0$  is the  $z'$  axis.

If we assume the Schwarzschild metric around the neutron star with mass  $M$  and radius  $R$ , the number flux, per photon energy  $E_{\infty}$ , of thermal photons emitted from the stellar surface and received by a distant observer may be given by (e.g., Page 1995)

$$\frac{1}{S} \frac{d^2 N(E_{\infty})}{dt_{\infty} dE_{\infty}} = \frac{2\pi}{c^2 h^3} \frac{R_{\infty}^2}{D^2} E_{\infty}^2 \int_0^1 2q dq \int_0^{2\pi} \frac{d\phi'}{2\pi} \frac{1}{e^{f e^{-\eta} E_{\infty}/k_B T} - 1} \equiv \frac{2\pi}{c^2 h^3} \frac{R_{\infty}^2}{D^2} \frac{E_{\infty}^2}{e^{-\eta} E_{\infty}/k_B T_0 - 1} G_{E_{\infty}}(t_{\infty}), \quad (8)$$

and integrating equation (8) with respect to the variable  $E_\infty$  leads to

$$\frac{1}{S} \frac{dN(E_\infty)}{dt_\infty} = 2.404 \times \frac{2\pi}{c^2 h^3} \frac{R_\infty^2}{D^2} \int_0^1 2q dq \int_0^{2\pi} \frac{d\phi'}{2\pi} \left( \frac{k_B T}{f e^{-\eta}} \right)^3 \equiv \frac{4.808\pi}{c^2 h^3} \frac{R_\infty^2}{D^2} \left( \frac{k_B T_0}{e^{-\eta}} \right)^3 G(t_\infty), \quad (9)$$

where  $D$  is the distance to the observer,  $T$  is the surface temperature,  $k_B$  is the Boltzmann constant,  $c$  is the velocity of light, and  $h$  is the Planck constant, and we have neglected, for simplicity, the interstellar absorption effect and the dependence of the effective area  $S$  of the detector on the photon energy. Here,

$$R_\infty = e^{-\eta} R \quad (10)$$

is the radius of the star seen by a distant observer, and  $dt_\infty = e^{-\eta} dt$  denotes the increment of the coordinate time  $t_\infty$ , where

$$e^\eta = \sqrt{1 - R_G/R} \quad (11)$$

and  $R_G = 2GM/c^2$  is the Schwarzschild radius, and  $dt$  is the increment of the proper time at the surface of the star. Note that  $\Omega_\infty = e^\eta \Omega$  since  $\Omega_\infty dt_\infty = \Omega dt$ , where  $\Omega_\infty$  is the angular spin frequency of the star seen from infinity. If we let  $E_e$  and  $E_\infty$  denote, respectively, the photon energy in the corotating frame of the star at the surface and the photon energy received by a distant observer, we have

$$E_e = f e^{-\eta} E_\infty, \quad (12)$$

where the factor  $f$ , representing the Doppler shift in the photon energy from  $e^{-\eta} E_\infty$  in the non-rotating frame at the stellar surface to  $E_e$  in the co-rotating frame, is given by

$$f = \gamma(1 - \mathbf{v} \cdot \mathbf{o}/c), \quad (13)$$

where  $\mathbf{v} = \boldsymbol{\Omega} \times \mathbf{R} = R\Omega \sin\theta \mathbf{e}_\phi$  with  $\mathbf{e}_\phi$  being the unit vector in the azimuthal direction and  $\mathbf{o}$  is the unit vector along the trajectory of a photon at the surface, and  $\gamma = 1/\sqrt{1 - v^2/c^2}$ . Note that the four vector of a photon in the non-rotating frame may be given by  $o^\mu = e^{-\eta} E_\infty(1, \mathbf{o})$ . Using the angle  $\zeta(\theta')$  between the local normal and the photon trajectory, at the surface, reaching the observer at infinity, the variable  $q$  in equations (8) and (9) is defined by

$$q \equiv \sin \zeta, \quad (14)$$

and the relation between  $\theta'$  and  $q$  is determined by the integration given by

$$\theta'(q) = \int_0^{R_G/2R} \frac{q du}{\sqrt{(1 - R_G/R) R_G/2R - (1 - 2u)u^2 q^2}}. \quad (15)$$

The maximum value  $\theta'_{\max}$  occurs when  $q = 1$  and is shown as a function of the radius  $R$  in Figure 1 for  $M = 1.4M_\odot$ . Since  $\mathbf{o}$  at the stellar surface is given by

$$\mathbf{o} = \sin(\theta' - \zeta) \cos \phi' \mathbf{i}' + \sin(\theta' - \zeta) \sin \phi' \mathbf{j}' + \cos(\theta' - \zeta) \mathbf{k}', \quad (16)$$

where  $\mathbf{i}'$ ,  $\mathbf{j}'$ , and  $\mathbf{k}'$  are the orthonormal vectors parallel to the  $x'$ ,  $y'$ , and  $z'$  axes, respectively, we have

$$\frac{\mathbf{v} \cdot \mathbf{o}}{\Omega R \sin \theta} = \sin(\theta' - \zeta) (\cos \phi \sin \phi' - \sin \phi \cos \phi' \cos i) - \cos(\theta' - \zeta) \sin \phi \sin i. \quad (17)$$

Note that without light bending so that  $\theta' = \zeta$ , we simply have  $\mathbf{v} \cdot \mathbf{o} = -\Omega R \sin \phi \sin i \sin \theta$ . The aberration effect may be given by

$$\cos \zeta_e = \frac{e^{-\eta} E_\infty}{E_e} \cos \zeta, \quad (18)$$

where  $\zeta_e$  is the angle measured in the corotating frame of the star.

For waves whose  $\phi$  and  $t$  dependence is given by  $e^{im\phi + i\sigma t}$ , it is easy to incorporate the time-delay effect that arises because of the difference in the path lengths of photons emitted from different points on the surface of the star. Since the travel time of a photon from a point having the impact parameter  $b = qR_\infty$  at the surface of the star to an observer at infinity is given by

$$t_\infty(b) = \frac{R_G}{c} \int_R^\infty \frac{1}{\sqrt{1 - (1 - R_G/r)(b/r)^2}} \left(1 - \frac{R_G}{r}\right)^{-1} \frac{dr}{R_G}, \quad (19)$$

the time-lag may be defined by

$$\Delta t_\infty(b) \equiv t_\infty(b) - t_\infty(0). \quad (20)$$

Replacing  $t_\infty$  by  $t_\infty - \Delta t_\infty(b)$ , we rewrite the time and  $\phi$  dependence  $e^{im\phi + i\sigma t}$  of the perturbations as

$$e^{im\phi + i\sigma t} e^{-ie^\eta \sigma \Delta t_\infty(b)} \quad (21)$$

**Table 1.** Oscillation frequencies  $\bar{\omega}$  and  $\bar{\sigma}/m$  for the fundamental ( $n = 0$ )  $r$ -modes for the mass-accreting envelope model with  $\dot{M} = 0.1\dot{M}_{\text{Edd}}$  for  $M = 1.4M_{\odot}$  and  $R = 10\text{km}$ . Here the frequencies  $\bar{\omega}$ ,  $\bar{\sigma}$ , and  $\bar{\Omega}$  are normalized by  $\sqrt{GM/R^3}$ .

$k$	$m$	$\bar{\Omega} = 0.2$		$\bar{\Omega} = 0.4$	
		$\bar{\omega}$	$\bar{\sigma}/m$	$\bar{\omega}$	$\bar{\sigma}/m$
0	1	5.31(-3)	-0.1947	5.31(-3)	-0.3947
	2	1.02(-2)	-0.1949	1.04(-2)	-0.3948
1	1	3.24(-3)	-0.1968	3.22(-3)	-0.3967
	2	6.32(-3)	-0.1968	6.36(-3)	-0.3968

so that we can take account of the time-lag effects in light curve calculations (see e.g., Cadeau et al. 2005).

For the light curves  $G(t)$  or  $G_{E_{\infty}}(t)$ , we calculate the discrete Fourier transform  $a_j$  ( $j = -N/2, \dots, N/2 - 1$ ) defined by

$$a_j = \sum_{k=0}^{N-1} G(t_k) e^{2\pi i f_j t_k} \quad (22)$$

where  $N$  is the total number of sampling points in the time span  $\Delta T$ , and  $t_k = k\Delta T/N$  and  $f_j = j/\Delta T$ , and  $|a_j| = |a_{-j}|$  for a real function  $G(t)$ . To indicate the amplitude of the light variation with the frequency  $f_j$ , we use the quantity defined by

$$A(\omega_j) = 2|a_j|/N, \quad (23)$$

where  $\omega_j = 2\pi f_j$ .

### 3 NUMERICAL RESULTS

The surface  $r$ -modes propagating in the fluid ocean of a rotating neutron star may be classified in terms of three quantum numbers ( $m, k, n$ ), where  $m$  is the azimuthal wave number around the rotation axis,  $k$  is the number of latitudinal nodes, and  $n$  is the number of radial nodes of the eigenfunctions. For the quantum number  $k$ , we count the latitudinal nodes of the eigenfunctions  $\text{Re}[\delta T(R, \theta)]$ , and for the quantum number  $n$  we count the radial nodes of the eigenfunction  $iT_{l_1}(r)$ . In this paper, we exclude the  $r$ -modes of  $l' = |m|$  for light curve calculations, since their frequency changes during bursts are much larger than is suggested by observations (e.g., Cumming & Bildsten 2000, Lee 2004). Then, the  $r$ -modes with the quantum number  $k = 0, 1, 2, \dots$  correspond to the  $r$ -modes of  $l' = |m| + 1, |m| + 2, |m| + 3, \dots$ , respectively, and the corotating frame frequency  $\omega$  decreases in this order for given  $m, n$ , and  $\Omega$ . The  $r$ -modes with even  $k$  are denoted ‘‘even’’ modes, and have eigenfunctions  $\delta T(R, \theta)$  that are symmetric about the equator of the star, while the  $r$ -modes with odd  $k$  are called ‘‘odd’’ modes and are antisymmetric about the equator.

For light curve calculations in this paper, we consider only the fundamental  $r$ -modes with no radial nodes ( $n = 0$ ) of the eigenfunction  $iT_{l_j}$ , because they are the most strongly excited in thermonuclear bursts (Lee 2004). In addition, since the  $r$ -modes associated with high  $m$  and  $k$  are unlikely to produce light variations with appreciable amplitudes, we restrict our numerical analysis to the fundamental modes with  $m = 1$  or  $m = 2$  and with  $k = 0$  or  $k = 1$ . Employing these simplifications, and assuming two  $r$ -modes with different  $m$  may be excited, we can express the surface temperature for light curve calculation as

$$T(R, \theta, \phi, t) = T_0 + \text{Re} \left[ C_1 \delta T^{\alpha_1}(R, \theta) e^{i(\phi + \sigma_{\alpha_1} t)} + C_2 e^{i\chi} \delta T^{\alpha_2}(R, \theta) e^{i(2\phi + \sigma_{\alpha_2} t)} \right], \quad (24)$$

where

$$\delta T^{\alpha_1}(R, \theta) = \sum_{j \geq 1} \delta T_{l_j}^{\alpha_1}(R) Y_{l_j}^1(\theta, 0), \quad \delta T^{\alpha_2}(R, \theta) = \sum_{j \geq 1} \delta T_{l_j}^{\alpha_2}(R) Y_{l_j}^2(\theta, 0), \quad (25)$$

and  $C_1 = C_{\alpha_1}$  and  $C_2 = C_{\alpha_2}$  are here real constants for the amplitudes of the modes, and  $\chi$  is a real parameter, giving the phase difference between the two  $r$ -modes. If we define  $\alpha = (m, k, n)$ , we have  $\alpha_1 = (1, 0, 0)$  and  $\alpha_2 = (2, 0, 0)$  for the even modes, and  $\alpha_1 = (1, 1, 0)$  and  $\alpha_2 = (2, 1, 0)$  for the odd modes. For the oscillation frequencies, we adopt the approximation that  $\sigma_{\alpha_1} = -\Omega$  and  $\sigma_{\alpha_2} = -2\Omega$ . The parameters we need to calculate the function  $G(t)$  defined by equation (9) are the mass  $M$ , the radius  $R$ , the angular rotation speed  $\Omega$  of the star, the oscillation amplitudes  $C_1$  and  $C_2$ , the phase difference  $\chi$  between the two modes, and the inclination angle  $i$ . For the function  $G_{E_{\infty}}(t)$  defined by equation (8), we need in addition the surface temperature  $T_0$  and the photon energy  $E_{\infty}$ .

For the  $r$ -mode calculation, we use a mass-accreting envelope model with the rate  $\dot{M} = 0.1\dot{M}_{\text{Edd}}$  for a neutron star having  $M = 1.4M_{\odot}$  and  $R = 10^6\text{cm}$ , where  $\dot{M}_{\text{Edd}} = 4\pi cR/\kappa_e$  with  $\kappa_e$  being the electron scattering opacity. This envelope model is a fully radiative model with no convective regions in it, and the detail of the envelope calculation is given in Strohmayer &

Lee (1996) and Lee (2004). To calculate the modes propagating in the mass-accreting envelope of a rotating neutron star, we follow the method described by Lee & Saio (1987, 1993). Note that the formulation employed for the envelope and oscillation mode calculations is Newtonian, and no general relativistic effects are included. In Table 1, the oscillation frequencies  $\bar{\omega}$  and  $\bar{\sigma}/m$  are tabulated for the fundamental  $r$ -modes with low  $m$  and  $k$  for  $\bar{\Omega} = 0.2$  and  $\bar{\Omega} = 0.4$ , where the frequencies  $\bar{\omega}$ ,  $\bar{\sigma}$ , and  $\bar{\Omega}$  are normalized frequencies by  $\sqrt{GM/R^3}$ . It is important to note that the corotating frame oscillation frequency  $\bar{\omega}$  is almost insensitive to  $\bar{\Omega}$  for rapidly rotating stars (Lee 2004), and that for a given  $k$  the inertial frame pattern speed  $\bar{\sigma}/m$  for  $m = 2$  is nearly equal to that for  $m = 1$ , which may justify the simplification of  $\sigma = -m\Omega$ . The temperature variations  $\delta T(R, \theta)/T_0$  caused by the surface  $r$ -modes for  $\bar{\Omega} = 0.2$  are shown in Figure 1, where panels (a) to (d) are for  $\alpha = (1, 0, 0)$ ,  $(2, 0, 0)$ ,  $(1, 1, 0)$ , and  $(2, 1, 0)$ , respectively, and the solid and the dashed lines denote respectively the real and imaginary parts of the function  $\delta T(R, \theta)/T_0$ . Here, the amplitude normalization is given by  $|\text{Re}[iT_{l_1}(R)/R]| = 1$  at the surface of the star. We note that the functions  $\delta T(R, \theta)/T_0$  and  $iT_{l_1}(R)/R$  have comparable amplitudes to each other at the stellar surface, and that the imaginary part of  $\delta T(R, \theta)/T_0$  is much smaller than the real part. The  $\theta$  dependence of the function  $\delta T(R, \theta)/T_0$  for the even (odd)  $r$ -mode with  $m = 1$  is quite similar to that for the even (odd)  $r$  mode with  $m = 2$  except for the fact that the maxima of the functions for  $m = 2$  are larger than those for  $m = 1$ . In this paper, the temperature perturbations  $\delta T(R, \theta)$  calculated for  $R = 10\text{km}$  will be used for different values of  $R$  for simplicity. Applying the approximation  $\sigma = -m\Omega$ , we have  $m\phi + \sigma_\alpha t = m\phi - m\Omega t$ , and we call the Fourier amplitudes  $A(\omega_j)$  at  $\omega_j = \Omega$  and  $\omega_j = 2\Omega$  the fundamental and the first harmonic components, respectively.

Since we are applying a linear theory of stellar pulsations, we cannot self-consistently determine the amplitudes of the modes, which forces us to treat the oscillation amplitudes as parameters in the modeling. For simplicity, we use  $C_1 = 0.2$  for  $m = 1$  and  $C_2 = 0.2$  for  $m = 2$  for the mode amplitudes throughout the following calculations. Since the toroidal component of the displacement vector is dominant for the  $r$ -modes, the velocity,  $v$ , of a surface fluid element may be approximately given by  $v \sim |\omega iT_{l_1}(R)| = R\sqrt{GM/R^3}|\bar{\omega}| \times |iT_{l_1}(R)/R|$ . Since  $|\bar{\omega}| \lesssim 0.01$ , we have the fluid velocity  $v \lesssim 10^{-3}c$  for  $|iT_{l_1}(R)/R| \sim 0.2$  if we adopt the stellar parameters  $M = 1.4M_\odot$  and  $R = 10\text{km}$ , for which  $R\sqrt{GM/R^3} \sim 0.5c$ . If we use the sound velocity  $v_s = k_B T/\mu H$  at the surface, we have  $v_s \sim 10^{-3}c$  for  $T = 10^7\text{K}$  and  $\mu = 0.5$ , where  $H$  and  $\mu$  denote the hydrogen mass and the mean molecular weight, respectively. For the value of  $C_1 = 0.2$  (or  $C_2 = 0.2$ ) for the amplitude parameter, the fluid velocity at the surface is much smaller than the velocity of light and is comparable to or less than the local sound velocity at the surface.

### 3.1 Light curves produced by a single $r$ -mode with low $m$

Since the imaginary part of  $\delta T(R, \theta)/T_0$  is much smaller than the real part, assuming that only a single  $r$ -mode of low  $m$  is excited, we may simply write the surface temperature as

$$T = T_0 [1 + C(\theta) \cos(m\phi - m\Omega t)], \quad (26)$$

where  $C(\theta) = \text{Re}[C_j \delta T(R, \theta)/T_0]$  and  $j = 1$  or  $j = 2$ . Note that setting the origins of times  $t$  and  $t_\infty$  appropriately, we can assume  $\Omega t = \Omega_\infty t_\infty$ . The function  $G(t)$  is given by

$$G(t) = G_0 + G_1^c \cos m\Omega t + G_1^s \sin m\Omega t + G_2^c \cos 2m\Omega t + G_2^s \sin 2m\Omega t + \dots, \quad (27)$$

where

$$G_0 = \int_0^1 2qdq \int_0^{2\pi} \frac{d\phi'}{2\pi} \frac{1 + 1.5C^2(\theta)}{f^3}, \quad (28)$$

$$G_1^c = \int_0^1 2qdq \int_0^{2\pi} \frac{d\phi'}{2\pi} 3f^{-3} C(\theta) \left[ 1 + \frac{C^2(\theta)}{4} \right] \cos m(\phi + \Delta\phi), \quad (29)$$

$$G_1^s = \int_0^1 2qdq \int_0^{2\pi} \frac{d\phi'}{2\pi} 3f^{-3} C(\theta) \left[ 1 + \frac{C^2(\theta)}{4} \right] \sin m(\phi + \Delta\phi), \quad (30)$$

$$G_2^c = \int_0^1 2qdq \int_0^{2\pi} \frac{d\phi'}{2\pi} \frac{3}{2} f^{-3} C^2(\theta) \cos 2m(\phi + \Delta\phi), \quad (31)$$

$$G_2^s = \int_0^1 2qdq \int_0^{2\pi} \frac{d\phi'}{2\pi} \frac{3}{2} f^{-3} C^2(\theta) \sin 2m(\phi + \Delta\phi), \quad (32)$$

where  $\Delta\phi = \Omega_\infty \Delta t_\infty(b)$ , and we have replaced  $t_\infty$  by  $t_\infty - \Delta t_\infty(b)$  to calculate the light curves at  $t_\infty$  at the observer. It may be important to note that the coefficients  $G_1^s$  and  $G_2^s$  vanish if we assume  $f = 1$  and  $\Delta\phi = 0$ . Equation (27) indicates that there appears a periodic component having the frequency  $2m\Omega$  unless  $G_2^c$  and  $G_2^s$  vanish simultaneously. The terms associated with the frequency  $m\Omega$ , for example, can be rewritten as

$$G_1^c \cos m\Omega t + G_1^s \sin m\Omega t = G_1 \cos(m\Omega t - \delta), \quad (33)$$

where  $G_1 = \sqrt{(G_1^c)^2 + (G_1^s)^2}$ ,  $\tan \delta = G_1^s/G_1^c$ , and the value of  $\Omega t = (\delta + 2n\pi)/m$  that maximizes the variation depends on the parameters  $R$  and  $i$ , where  $n$  is an integer. Since the imaginary part of  $\delta T(T, \theta)$  is negligible compared with the real part, we have in a good approximation

$$A(m\Omega) = G_1, \quad A(2m\Omega) = G_2, \quad (34)$$

where  $G_2 = \sqrt{(G_2^c)^2 + (G_2^s)^2}$ , and the Fourier amplitude  $A(\omega_j)$  is defined by equation (23). If we define the phase shift  $\delta_j$ , using the Fourier transform  $a_j$  given in equation (22), as

$$\tan \delta_j = \text{Im}(a_j)/\text{Re}(a_j), \quad (35)$$

we have to good approximation  $\delta = \delta_j$ , selecting the integer  $j$  so that  $2\pi f_j = m\Omega$ .

The quantities  $G_1$  and  $\delta/(2m\pi)$  defined by equation (33) are plotted as a function of the inclination angle  $i$  for the even ( $k=0$ )  $r$ -mode with  $m=1$  in Figure 3, and for the even ( $k=0$ )  $r$ -mode with  $m=2$  in Figure 4, where we assume  $\bar{\Omega} = 0.2$ , and the dotted, short-dashed, solid, long-dashed, and dot-dashed lines indicate the radius  $R = 8, 9, 10, 15,$  and  $20\text{km}$ , respectively. The amplitude  $G_1$  vanishes at  $i=0$  because the temperature variations are proportional to  $e^{im\phi}$  where  $\phi = \phi'$  for  $i=0$ . For given  $i$  and  $R$ , the amplitude  $G_1$  for  $m=1$  is usually larger than that for  $m=2$ . For a given inclination angle  $i$ , the amplitude  $A(m\Omega) = G_1$  decreases as the radius  $R$  decreases. This is because the maximum angle  $\theta'_{\text{max}}$  increases with decreasing  $R$  so that almost the whole surface area of the star can be seen at any time by the distant observer. For the even modes, the amplitude  $G_1$  for a given  $R$  monotonically increases with increasing  $i$ . As shown by Figures 3 and 4 the phase shift  $\delta/(2m\pi)$  for the even  $r$ -modes are negative. The absolute value  $|\delta/(2m\pi)|$  for  $m=1$ , which stays small, increases with decreasing  $R$ , and it is rather insensitive to the inclination angle  $i$  for a given  $R$ . The absolute value  $|\delta/(2m\pi)|$  for  $m=2$  also increases as  $R$  decreases and becomes as large as  $|\delta/(2m\pi)| \sim 0.2$  for the smallest  $R$  considered here. It shows a weak dependence on  $i$ , particularly for the radii  $R \sim 10\text{km}$ .

The quantities  $G_1$  and  $\delta/(2m\pi)$  are given as a function of the inclination angle  $i$  for the odd ( $k=1$ )  $r$ -mode with  $m=1$  in Figure 5, and for the odd ( $k=1$ )  $r$ -mode with  $m=2$  in Figure 6, where  $\bar{\Omega} = 0.2$ , and the different curves have the same meaning as in Figure 3. For the odd modes, the amplitude  $G_1$  vanishes at  $i=90^\circ$  also, because the temperature variation pattern is antisymmetric about the equator of the star. As in the case of the even  $r$ -modes, the amplitude  $G_1$  for the odd  $r$ -modes decreases with decreasing  $R$  for a given  $i$ . Although  $\delta/(2m\pi)$  for larger radii  $R \gtrsim 15\text{km}$  stays constant with varying  $i$ , it shows a strong dependence on  $i$  for smaller radii  $R \lesssim 10\text{km}$ .

Figure 7 shows the amplitude ratio  $G_2/G_1$  for the even  $r$ -mode with  $m=1$  (upper panel) and for the odd  $r$ -mode with  $m=1$  (lower panel) as a function of  $i$ . We find the ratio is at most of order  $\sim 0.01$  for the even  $m=1$   $r$ -modes, which indicates that the first harmonic component cannot be significant in the light curves produced by a single even  $r$ -mode of low  $m$ . For the odd  $m=1$   $r$  mode, on the other hand, the first harmonic component has appreciable amplitude compared to the fundamental, particularly when  $i \sim 90^\circ$ . Actually, the ratio  $G_2/G_1$  diverges as  $i$  increases to  $90^\circ$ .

As examples, we show as a function of  $\Omega t/2\pi$  the light curves produced by the even,  $m=1$   $r$ -mode in Figure 8, and by the odd,  $m=1$   $r$ -mode in Figure 9, where we assume  $\bar{\Omega} = 0.2$  and  $i = 60^\circ$ . Figure 10 shows the light curves generated by the odd,  $m=1$   $r$ -mode as a function of  $\Omega t/2\pi$  for  $\bar{\Omega} = 0.2$  and  $R = 10\text{km}$ , where the dotted, short-dashed, solid, long-dashed, and dot-dashed lines indicate the inclination angle  $i = 10^\circ, 30^\circ, 50^\circ, 70^\circ,$  and  $90^\circ$ , respectively. At  $i = 90^\circ$ , only the first harmonic component associated with  $2m\Omega$  appears.

### 3.2 Dependence on $\bar{\Omega}$

As  $\Omega$  increases, the amplitudes of the  $r$ -modes are more strongly confined to the equatorial region of the star, which makes the amplitude  $G_1$  larger for the even  $r$ -modes but smaller for the odd modes. Note that the frequency  $\omega$  is only weakly dependent on  $\Omega$  for the modes. To see the effects of rapid rotation, we calculate  $G_1$  and  $\delta$  for the even,  $m=1$   $r$ -mode for  $\bar{\Omega} = 0.4$ , and we plot the results in Figure 11, where the different curves represent different radii as in Figure 3. We note that the magnitude of the phase shift  $\delta$  is larger for  $\bar{\Omega} = 0.4$  than for  $\bar{\Omega} = 0.2$  although  $\delta$  is still only weakly dependent on the inclination angle  $i$  for the mode.

### 3.3 Light curves produced by two $r$ -modes

Although the even,  $m=1$   $r$ -mode will produce the largest light variations of the modes considered here, the mode is not likely to produce a first harmonic component  $A(2\Omega)$  of appreciable strength. In order to account for observed light curves that contain a substantial first harmonic component, we may need to assume that the  $r$ -modes with  $m=1$  and  $m=2$  are excited simultaneously. As an example, we calculate the light curves  $G(t)$  produced by the two simultaneously excited even  $r$ -modes with  $m=1$  and  $m=2$ , assuming  $C_1 = C_2 = 0.2$ ,  $\chi = 0$ ,  $i = 90^\circ$ , and  $\bar{\Omega} = 0.2$ . We plot  $G(t)$  as a function of  $\Omega t/2\pi$  in

Figure 12 and the Fourier amplitudes  $A(\Omega)$  and  $A(2\Omega)$  as a function of the radius  $R$  in Figure 13, where the different curves in Figure 12 have the same meaning as in Figure 3. Obviously, using two  $r$ -modes with different  $m$ 's, we can produce a variety of light curves, including those with a harmonic content similar to that seen from XTE J1814-338 (Strohmayer et al. 2003). It is important to note that, even if we abandon the simplification given by  $\sigma_{\alpha_1} = -\Omega$  and  $\sigma_{\alpha_2} = -2\Omega$ , we have in a good approximation  $2\sigma_{\alpha_1} = \sigma_{\alpha_2}$  as shown by Table 1.

### 3.4 Phase Lags

The amplitudes of the light curves produced by the surface  $r$ -modes are inevitably related to the parameters  $C_i$ 's as well as to the ratio  $R/M$ . Since the oscillation amplitudes are difficult to determine within the framework of a linear theory of stellar pulsations and the ratio  $R/M$  itself is one of our main parameters to determine observationally, it would be useful to find an additional observable that can be used as an indicator for the ratio  $R/M$ . Considering the even  $r$ -mode with  $m = 1$ , which is most likely to be responsible for the light variations, we note that the phase shift  $\delta$ , which is almost independent of the oscillation amplitude parameter  $C_1$ , is rather insensitive to the inclination angle  $i$  but is almost a monotonic function of the radius  $R$  (i.e., the ratio  $R/M$ ) for a given  $i$ . If it is true that the observed light variations during burst oscillations are caused by an even,  $m = 1$   $r$ -mode, it would be possible to use the phase shift  $\delta$  as an indicator for the ratio  $R/M$ . To derive an observable using the phase shift  $\delta$ , we calculate the function  $G_{E_\infty}(t)$  defined in equation (8) for appropriate values of  $T_0$  and  $E_\infty$ , and Fourier analyze the function  $G_{E_\infty}(t)$  to obtain the phase shift  $\delta_j$  at  $\omega_j = \Omega$  using equation (35), which we denote  $\delta_E$ . In Figure 14, we plot as a function of the inclination angle  $i$  the difference  $\delta - \delta_{E_0}$  for the even,  $m = 1$   $r$ -mode (upper panel) and for the odd,  $m = 1$   $r$ -mode (lower panel) where we have assumed  $\bar{\Omega} = 0.2$ ,  $E_\infty = E_0 = 1\text{keV}$ ,  $k_B T_0 = 2.3\text{keV}$ , and the various curves represent different radii as in Figure 3. Since the difference  $\delta - \delta_{E_0}$  for the even  $r$ -mode with  $m = 1$  is almost insensitive to  $i$  and its magnitude increases almost monotonically with the radius  $R$  for a given  $i$ , the difference may be useful as an observational indicator for the ratio  $R/M$ . On the other hand, the difference for the odd mode shows a strong dependence on  $i$  for the radius  $R \lesssim 10\text{km}$ . Since the phase shifts  $\delta$  found in this paper are due mainly to the Doppler effects associated with rapid rotation of the star, the magnitude of the difference will be large for higher  $\bar{\Omega}$  for given  $M$  and  $R$ .

As shown in Figure 14, the phase difference,  $\delta - \delta_{E_0}$ , for the even mode is always negative, but that for the odd mode can be positive for radii  $R \lesssim 10\text{km}$ . Here, negative and positive values of  $\delta - \delta_{E_0}$  indicate hard leads and lags, respectively, for  $E_\infty = E_0 = 1\text{keV}$  and  $k_B T_0 = 2.3\text{keV}$ . To compare with observations more directly, it is convenient to give the phase shift difference,  $\delta_E - \delta_{E_0}$ , between the phase for  $E_\infty = E$  and that for a particular  $E_\infty = E_0$ . Examples are given as a function of the photon energy  $E$  in Figure 15 for the even  $r$ -mode with  $m = 1$  for  $i = 60^\circ$  and in Figure 16 for the odd  $r$ -mode with  $m = 1$  for  $i = 30^\circ$  (upper panel) and for  $i = 60^\circ$  (lower panel), where we have used  $E_0 = 1\text{keV}$  and  $\Omega_\infty/2\pi = 400\text{Hz}$ . For the even mode we always have negative  $\delta_E - \delta_{E_0}$ , indicating hard leads (soft lags), as suggested by Figure 14. On the other hand, for the odd  $m = 1$   $r$ -mode, we have both hard leads (soft lags) and hard lags, the latter of which occur at smaller radii (i.e., smaller  $R/M$ ). Observationally, there is an indication for hard lags during some burst oscillations, however, others are consistent with no phase variations with energy (Muno et al. 2003). Since the even,  $m = 1$   $r$ -mode generates hard leads (as the hot spot model does), our results suggest that a single even  $r$ -mode is probably inconsistent with burst oscillations which show hard lags. However, it might be possible for an oscillation produced by contributions from both even and odd modes to match the observed phase lag properties of burst oscillations. We will explore detailed modeling and fitting, including the effects of the detection process, in a subsequent paper.

## 4 DISCUSSION

The surface  $r$ -modes considered in this paper belong to a subclass of the equatorial waves (Pedlosky 1987). In the equatorial  $\beta$  plane approximation, we employ a Cartesian coordinate system in which the coordinate origin is at the equator and the  $x$ ,  $y$ , and  $z$  axes are in the eastward, northward, and upward directions, respectively. The wave equations in the  $\beta$  plane approximation are solved by applying the method of separation of variables, in which a separation constant  $\lambda$  is introduced between  $(x, y, t)$  and  $z$ . The separation constant  $\lambda$  is an eigenvalue that is determined by solving the wave equation in the vertical direction with appropriate boundary conditions, and reflects the vertical structure of the thin fluid envelope. Assuming the perturbed velocity  $v'_y(x, y, z, t)$  is given by  $v'_y \propto e^{i(kx + \omega t)} \Psi(y) V(z)$ , we obtain for the equatorial waves the dispersion relation given by (Pedlosky 1987)

$$\lambda \tilde{\omega}^2 + \tilde{k}/\tilde{\omega} - \tilde{k}^2 = (2j + 1)\sqrt{\lambda}, \quad (36)$$

where

$$\tilde{\omega} = \omega/(\beta_0 L_e), \quad \tilde{k} = L_e k, \quad L_e = \sqrt{N_0 D/\beta_0}, \quad \beta_0 = 2\Omega/R, \quad (37)$$

and  $N_0$  is a characteristic value of the Brunt-Väisälä frequency,  $D$  is the depth of the fluid ocean, and the function  $\Psi(y)$  is given by



$$\Psi(y) = \psi_j(\tau) \equiv e^{-\tau^2/2} H_j(\tau) / \sqrt{2^j j! \pi^{1/2}}, \quad (38)$$

where  $H_j(\tau)$  is the Hermite polynomial,  $\tau = \lambda^{1/4} y / L_e$ , and  $j$  is an integer. Here, the function  $V(z)$  is determined by the wave equation in the vertical direction. The pressure perturbation for the equatorial waves for  $j \geq 1$  is then given by (Pedlosky 1987)

$$p'(x, y, z, t) = -\text{Re} \left\{ \frac{iA_j}{\lambda^{3/4}} \left[ -\left(\frac{j}{2}\right)^{1/2} \frac{\psi_{j-1}(\tau)}{\bar{\omega} - \bar{k}/\sqrt{\lambda}} + \left(\frac{j+1}{2}\right)^{1/2} \frac{\psi_{j+1}(\tau)}{\bar{\omega} + \bar{k}/\sqrt{\lambda}} \right] e^{i(kx + \omega t)} V(z) \right\}, \quad (39)$$

where  $A_j$  is an arbitrary constant. Since the low frequency equatorial waves at rapid rotation have (Lee 2004)

$$\omega \sim \frac{mN_0 D/R}{(2j+1)\sqrt{\lambda}}, \quad (40)$$

where we have assumed  $k \sim m/R$ ,  $p'(x, y, z, t)$  reduces to for  $j = 1$

$$p'(x, y, z, t) \sim -\text{Re} \left\{ \frac{3}{2\sqrt{2}\pi^{1/4}} \frac{iA_1}{\lambda^{1/4} L_e k} \left( \tau^2 + \frac{1}{2} \right) e^{-\tau^2/2} e^{i(kx + \omega t)} V(z) \right\}, \quad (41)$$

and for  $j = 2$

$$p'(x, y, z, t) \sim -\text{Re} \left\{ \frac{5}{3\sqrt{2}\pi^{1/4}} \frac{iA_2}{\lambda^{1/4} L_e k} \tau^3 e^{-\tau^2/2} e^{i(kx + \omega t)} V(z) \right\}. \quad (42)$$

Knowing that the perturbed potential temperature  $\Theta'$  is approximately given by  $\Theta' = \partial p' / \partial z$  (Pedlosky 1987), we find that the latitudinal ( $y$ ) dependence of  $\Theta'(x, y, z, t)$  well reproduces that of  $\delta T(R, \theta) / T_0$  in Figure 2 both for the even  $r$ -modes ( $j = 1$ ) and for the odd  $r$ -modes ( $j = 2$ ). Note that the solutions having the frequency (40) correspond to the type 2 solutions discussed by Longuet-Higgins (1968).

The oscillation energy  $E_W$  of a mode observed in the corotating frame may be given by (e.g., Unno et al. 1989)

$$E_W = \frac{\omega^2}{2} \int_{\Delta M_e} \boldsymbol{\xi} \cdot \boldsymbol{\xi}^* dM_r = \bar{\omega}^2 \frac{GM \Delta M_o}{R}, \quad (43)$$

where

$$\Delta M_o = \frac{1}{2} \int_{\Delta M_e} \frac{\boldsymbol{\xi} \cdot \boldsymbol{\xi}^*}{R^2} dM_r, \quad (44)$$

and  $\boldsymbol{\xi}^*$  is the complex conjugate of  $\boldsymbol{\xi}$ , and  $\Delta M_e$  is the envelope mass. If we let  $\Delta E_b$  and  $\Delta E_p$  denote the energies released during a burst and a persistent phase, respectively, we may assume  $\alpha \equiv \Delta E_p / \Delta E_b \sim 10^2$  and  $\Delta E_p \sim \epsilon GM \Delta M_a / R$ , where  $\epsilon \sim 0.1$  is a factor representing the efficiency of energy transformation from gravitational to radiation energies and  $\Delta M_a = \dot{M} \Delta t_p$  with  $\dot{M} \sim 10^{16} \text{gs}^{-1}$  being a typical mass accretion rate in close binary systems is the amount of mass accreting during the persistent phase  $\Delta t_p \sim 10^4 \text{s}$  (see, e.g., Frank, King, & Raine 2002). We then have

$$E_W = \alpha \epsilon^{-1} \bar{\omega}^2 (\Delta M_o / \Delta M_a) \Delta E_b, \quad (45)$$

which may be rewritten with appropriate normalization as

$$E_W \sim 2 \times \frac{\alpha}{100} \left( \frac{\epsilon}{0.1} \right)^{-1} \left( \frac{\dot{M}}{5 \times 10^{-18} M_\odot \text{s}^{-1}} \right)^{-1} \left( \frac{\Delta t_p}{10^4 \text{s}} \right)^{-1} \left( \frac{\bar{\omega}}{0.01} \right)^2 \left( \frac{C}{0.1} \right)^2 \frac{\langle \Delta M_o \rangle}{10^{-10} M_\odot} \Delta E_b, \quad (46)$$

where we have defined

$$\langle \Delta M_o \rangle = \frac{1}{2} \int_{\Delta M_e} \frac{\bar{\boldsymbol{\xi}} \cdot \bar{\boldsymbol{\xi}}^*}{R^2} dM_r, \quad (47)$$

assuming  $\boldsymbol{\xi} = C \bar{\boldsymbol{\xi}}$  with  $\bar{\boldsymbol{\xi}}$  being the displacement vector normalized as  $|\text{Re}[iT'_1(R)/R]| = 1$ . For the  $r$ -modes discussed in this paper, we have the ratio  $\langle \Delta M_o \rangle / 10^{-10} M_\odot \sim 0.1$  for the even  $r$ -modes, and  $\langle \Delta M_o \rangle / 10^{-10} M_\odot \sim 0.01$  for the odd  $r$ -modes, for  $\Omega = 0.2$  and  $\Delta M_e = 10^{-10} M_\odot$ . Although the estimation given above contains many parameters, all of which are not necessarily well determined, we may expect that the amount of energy required to excite the modes to appreciable amplitudes is a modest fraction of that released in a burst. It is interesting to note that, although the odd  $r$ -modes need to have larger amplitudes to produce appreciable light variations than the even  $r$ -modes, the former are easier to excite than the latter for a given amount of energy released in a burst.

## 5 CONCLUSIONS

We have calculated light curves produced by the surface  $r$ -modes of a rotating neutron star, taking account of the effects of gravitational light bending, gravitational red shift, and the difference in the arrival times of photons traveling in the

static Schwarzschild spacetime, as well as the Doppler shift of photon energy due to rapid spin of the star. We find that the fundamental even  $r$ -mode with  $m = 1$  produces the largest light variations. The light curves produced by a single even  $r$ -mode of a given  $m$  are dominated by the fundamental component with frequency  $m\Omega$ , although those produced by a single odd  $r$ -mode also contain a first harmonic component of appreciable amplitude as well as the fundamental component, the relative strengths depending on the inclination angle  $i$ . The phase shift  $\delta - \delta_{E_0}$  produced by the even  $m = 1$   $r$ -mode is only weakly dependent on the inclination angle  $i$  and is almost a monotonic function of  $R$  for a given  $i$ . The phase shift produced by the even  $r$ -mode with  $m = 1$  is a hard lead. The phase shift produced by the odd,  $m = 1$   $r$ -mode, on the other hand, depends both on  $i$  and on  $R$ , and there exists a parameter space of  $R$  and  $i$  which produces hard lags.

It is useful to translate the phase shift difference into a hard-lag measure,  $\Delta t_{\text{Lag}}$ , which is given for  $\Omega_\infty/2\pi = 400\text{Hz}$  by

$$\Delta t_{\text{Lag}} = \frac{2\pi}{\Omega_\infty} \frac{\delta_E - \delta_{E_0}}{2m\pi} = 2.5 \times \frac{\delta_E - \delta_{E_0}}{2m\pi} \quad \text{ms}, \quad (48)$$

where negative  $\Delta t_{\text{Lag}}$  means hard leads. As indicated by Figure 15, to fit the observed hard leads  $\sim -200\mu\text{s}$  at  $E_\infty \sim 10\text{keV}$  for SAX J1808.4-3658 (Cui et al. 1998) in terms of the *even*  $m = 1$   $r$ -mode we need a little bit smaller values of the ratio  $R/M$ . In fact, Weinberg et al. (2001) have assumed  $M = 2.2M_\odot$  and  $R = 10\text{km}$  for their fit, which is equivalent to  $R/R_G = 1.54$ , the value of which is substantially smaller than the smallest value  $R/R_G = 1.94$  for  $M = 1.4M_\odot$  and  $R = 8\text{km}$  we use in this paper. As suggested by Figure 16, however, the phase shift difference produced by the *odd*  $m = 1$   $r$ -mode may give a consistent value  $\sim -200\mu\text{s}$  at  $E_\infty \sim 10\text{keV}$  for  $M = 1.4M_\odot$ ,  $R = 10\text{km}$ , and  $i = 60^\circ$ , although the strong saturation of  $\Delta t_{\text{Lag}}$  above  $E \gtrsim 10\text{keV}$  is not necessarily well reproduced.

Compared with the hot spot model, the wave model generally produces smaller amplitude light variations. This is mainly because the entire surface of the neutron star produces X-ray emission. On the other hand, purely sinusoidal light curves observed for most of the burst oscillators (Muno et al. 2002b) can be explained by assuming the dominance of a single  $r$ -mode of a given  $m$ , and the existence of an appreciable first harmonic component may be attributable to the coexistence of a mode with  $2m$ , or perhaps a superposition of even and odd modes of different amplitude. As in the case of the hot spot model, the wave model also gives hard leads in most of the parameter space, which may be in conflict with the suggested hard lags seen in some of the burst oscillators, but might be applicable to the hard leads observed from the millisecond X-ray pulsars SAX J1808.4-3658, and IGR J00921+5934 (e.g., Cui et al. 1998; Galloway et al. 2005). The parameters employed in the light curve calculation include the mass  $M$ , the radius  $R$ , and the spin frequency  $\Omega$  of the star, the inclination angle  $i$ , the mode indices  $(m, k, n)$ , and the oscillation amplitudes  $C_j$ . Even if we assume that only the fundamental  $n = 0$   $r$ -modes with  $k = 0$  or  $k = 1$  play a role in producing the observed brightness variations and that the frequency that appears in the light curves is the spin frequency of the star, we still have several free parameters that affect the amplitude determination of the light curves. Perhaps the most crucial parameters are the oscillation amplitudes,  $C_j$ , themselves, which are difficult to determine within the framework of linear pulsation theory. Further theoretical studies combined with model fitting to the observed properties of burst oscillations will be definitely desired for a better understanding of the burst oscillations and the underlying neutron stars.

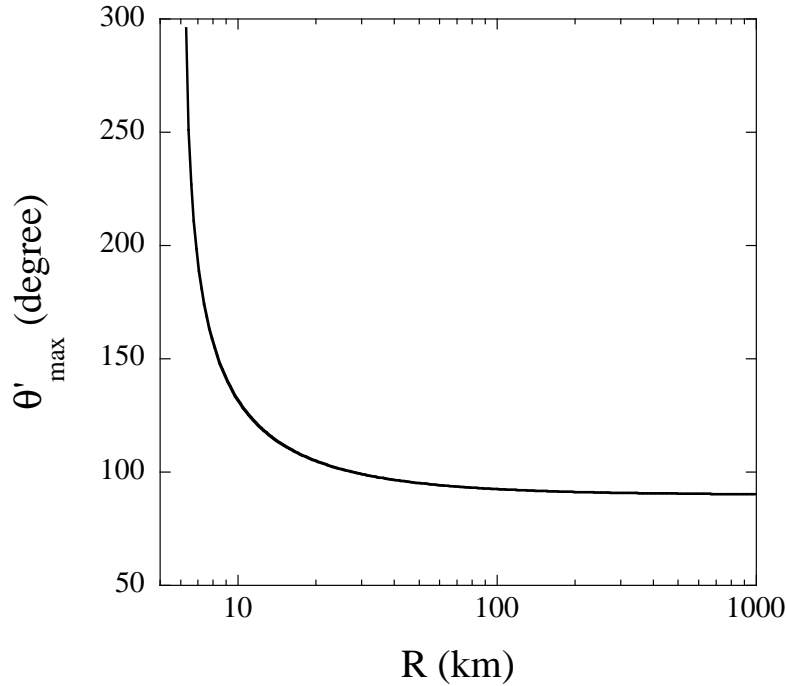


**Figure 1.**  $\theta'_{\max}$  as a function of the radius  $R$  for the star with the mass  $M = 1.4M_{\odot}$

## REFERENCES

- Bhattacharyya, S., Strohmayer, T.E., Miller, M.C., & Markwardt, C.B. 2005, *ApJ*, 619, 483
- Braje, T.M., Romani, R.W., & Rauch, K.P. 2000, *ApJ*, 531, 447
- Cadeau, C., Leahy, D.A., & Morsink, S.M. 2005, *ApJ*, 618, 451
- Chakrabarty, D., Morgan E.H., Munro, M.P., Galloway, D.K., Wijnands, R., van der Klis, M., & Markwardt, C.B. 2003, *Nature*, 424, 42
- Chen, K., & Shaham, J. 1989, *ApJ*, 339, 279
- Cui, W., Morgan, E.H., & Titarchuk, L.G. 1998, *ApJ*, 504, L27
- Cumming, A., & Bildsten, L. 2000, *ApJ*, 544, 453
- Cumming, A., Morsink, S.M., Bildsten, L., Friedman, J.L., & Holz, D.E. 2002, *ApJ*, 564, 343
- Ford, E.C. 1999, *ApJ*, 519, L73
- Frank, J., King, A., & Raine, D. 2002, *Accretion Power in Astrophysics* (3rd ed.; Cambridge: University of Cambridge Press)
- Galloway, D.K., Markwardt, C.B., Morgan, E.H., Chakrabarty, D., & Strohmayer, T.E. 2005, *astro-ph/0501064*
- Gierliński, M., Done, C., & Barret, D. 2002, *MNRAS*, 331, 141
- Heyl, J.S. 2004, *ApJ*, 600, 939
- Lee, U. 2004, *ApJ*, 600, 914
- Lee, U., & Saio, H. 1987, *MNRAS*, 225, 643
- Lee, U., & Saio, H. 1993, *MNRAS*, 261, 415
- Longuet-Higgins, M.S. 1968, *Phil. Trans. R. Soc.*, 262, 511
- Miller, M.C., & Lamb, F.K. 1998, *ApJ*, 499, L37
- Munro, M.P., Chakrabarty, D., & Galloway, D.K. 2002a, *ApJ*, 580, 1048
- Munro, M.P., Özel, F., & Chakrabarty, D. 2002b, *ApJ*, 581, 550
- Munro, M.P., Özel, F., & Chakrabarty, D. 2003, *ApJ*, 595, 1066
- Nath, T.R., Strohmayer, T.E., & Swank, J.H. 2002, *ApJ*, 564, 353
- Page, D. 1995, *ApJ*, 442, 273
- Pechenick, K.R., Ftaclas, C., & Cohen, J.M. 1983, *ApJ*, 274, 846
- Pedlosky, J. 1987, *Geophysical Fluid Dynamics* (2d ed.; New York: Springer)
- Poutanen, J., & Gierliński, M. 2003, *MNRAS*, 343, 1301
- Spitkovsky, A., Levin, Y., & Ushomirsky, G. 2002, *ApJ*, 566, 1018
- Strohmayer, T.E. 1992, *ApJ*, 388, 138
- Strohmayer, T.E., & Bildsten, L. 2004, in *Compact Stellar X-Ray Sources*, ed. W.H.G. Lewin & M. van der Klis (Cambridge: Cambridge Univ. Press)
- Strohmayer, T.E., Jahoda, K., Giles, B.A., & Lee, U. 1997, *ApJ*, 486, 355
- Strohmayer, T.E., & Lee, U. 1996, *ApJ*, 467, 773
- Strohmayer, T.E., & Markwardt, C.B. 1999, *ApJ*, 516, L81
- Strohmayer, T.E., Markwardt, C.B., Swank, J.H., & in'T Zand, J. 2003, *ApJ*, 596, L67
- Strohmayer, T.E., Zhang, W., Swank, J.H., White, N.E., & Lapidus, I. 1998a, *ApJ*, 498, L135
- Strohmayer, T.E., Zhang, W., Swank, J.H., & Lapidus, I. 1998b, *ApJ*, 503, L147
- Strohmayer, T.E., Zhang, W., Swank, J.H., Smale, A., Titarchuk, L., Day, C., & Lee, U. 1996, *ApJ*, 469, L9

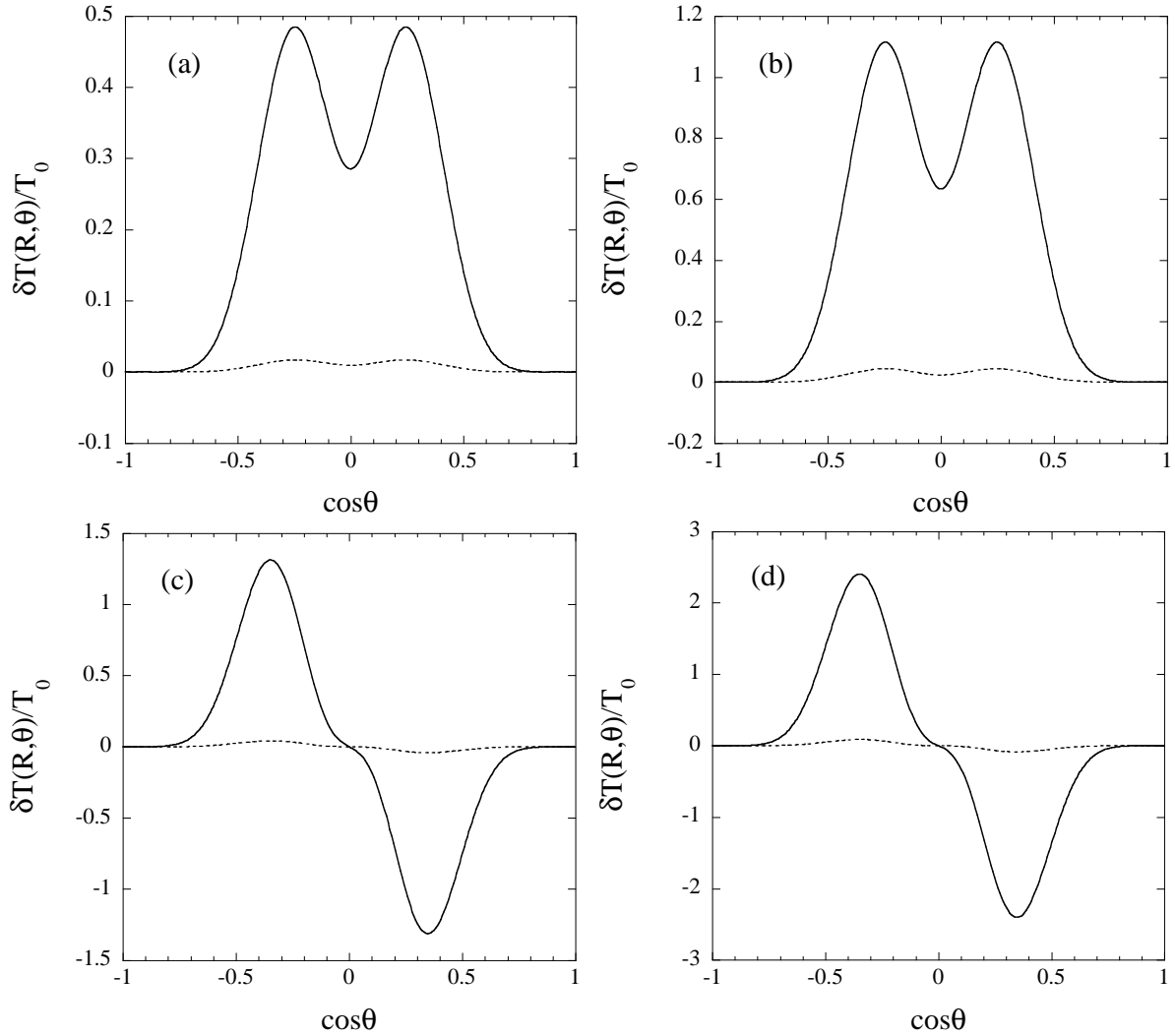


**Figure 2.**  $\delta T(R, \theta)/T_0$  as a function of  $\cos \theta$  for  $\bar{\Omega} = 0.2$ . Panel (a) for the fundamental even  $r$ -mode with  $m = 1$ , (b) for the fundamental even  $r$ -mode with  $m = 2$ , (c) for the fundamental odd  $r$ -mode with  $m = 1$ , (d) for the fundamental odd  $r$  mode with  $m = 2$ , where the solid and the dotted lines indicate the real and the imaginary parts, respectively. Here, the amplitude normalization for the mode is given by  $|\text{Re}[iT_{l_1}(R)/R]| = 1$  at the surface.

Unno, W., Osaki, Y., Ando, H., Saio, H., & Shibahashi, H. 1989, *Nonradial Oscillations of Stars* (2nd ed.; Tokyo: University of Tokyo Press)

van der Kils, M. 2004, [astro-ph/0410551](https://arxiv.org/abs/astro-ph/0410551)

Weinberg, N., Miller, M.C., & Lamb, D.Q. 2001, *ApJ*, 546, 1098

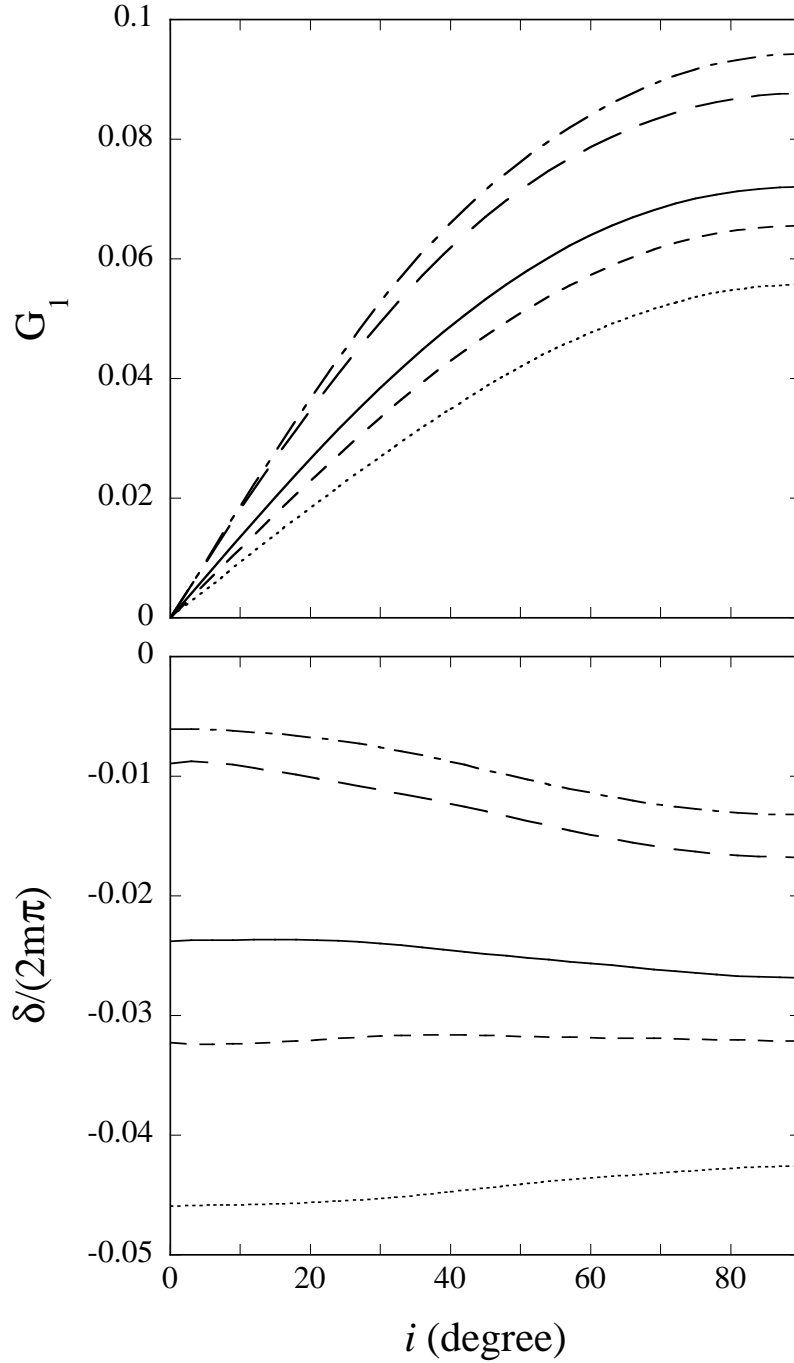


**Figure 3.** Amplitude  $G_1$  and phase shift  $\delta$  as a function of the inclination angle  $i$  for the fundamental even  $r$ -mode with  $m = 1$  ( $C_1 = 0.2$ ,  $C_2 = 0$ , and  $\chi = 0$ ), where  $\bar{\Omega} = 0.2$ , and the dotted, short-dashed, solid, long-dashed, and dash-dotted lines are for the radii  $R = 8, 9, 10, 15$ , and  $20$  km, respectively. Here, the amplitude normalization for the mode is given by  $|\text{Re}[iT_{l_1}(R)/R]| = 1$  at the surface.

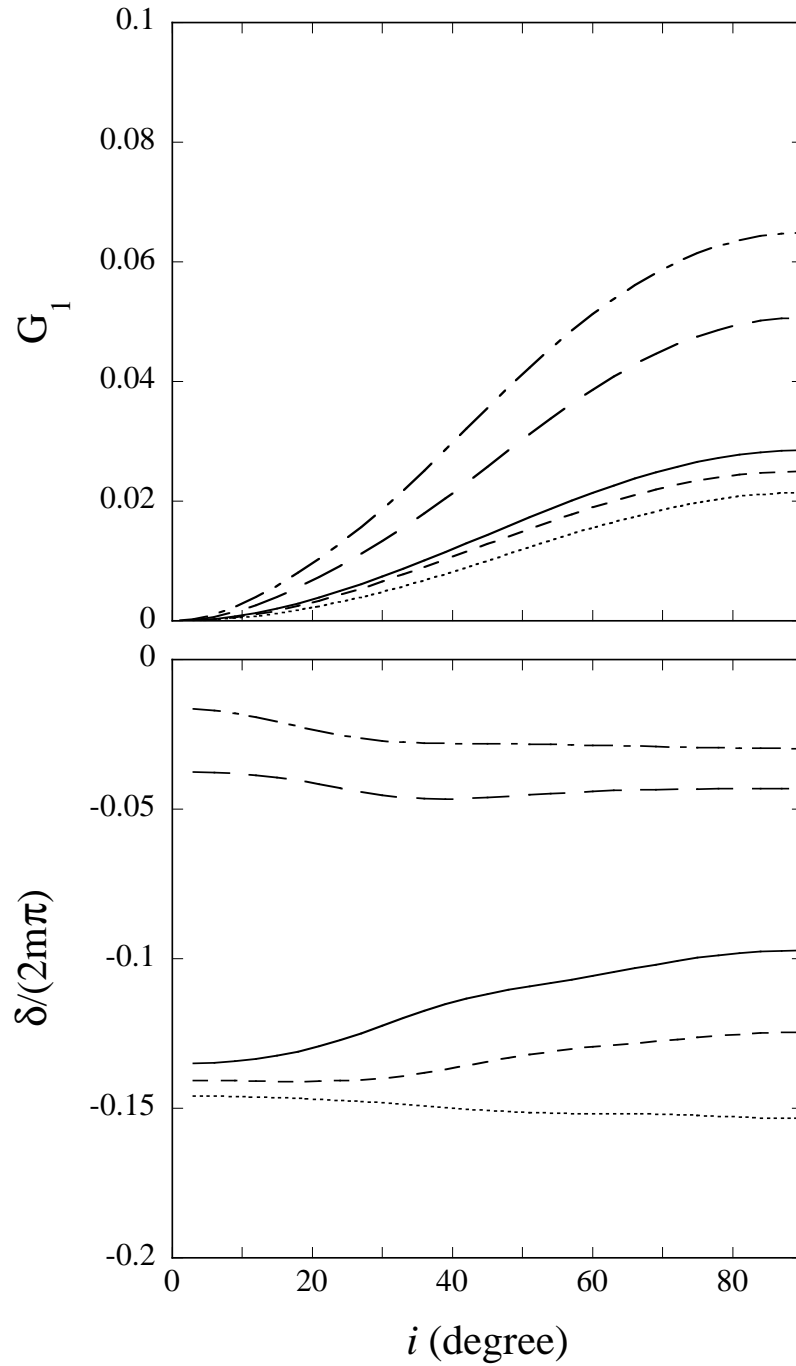


**Figure 4.** Same as Figure 3 but for the fundamental even  $r$ -mode with  $m = 2$  ( $C_1 = 0$ ,  $C_2 = 0.2$ , and  $\chi = 0$ ).

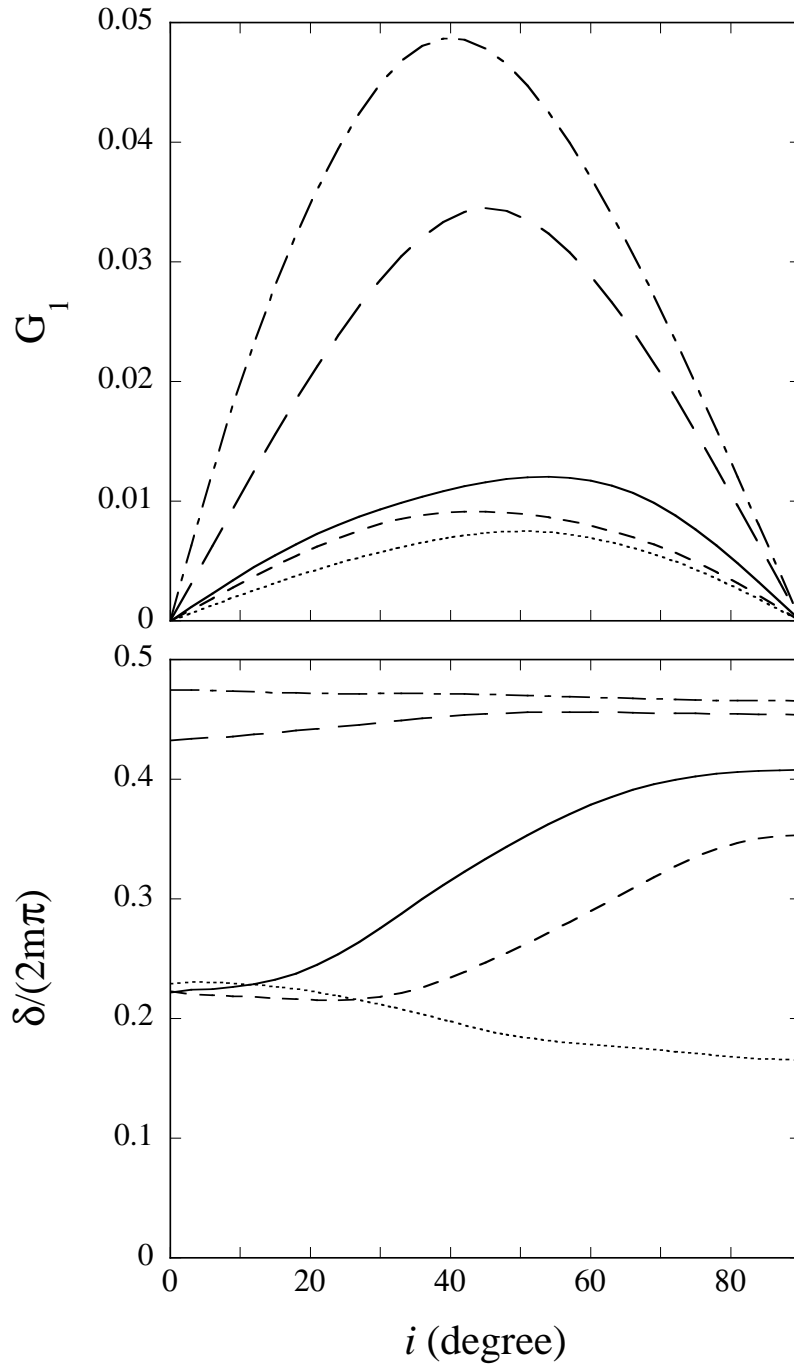


**Figure 5.** Same as Figure 3 but for the fundamental odd  $r$ -mode with  $m = 1$  ( $C_1 = 0.2$ ,  $C_2 = 0$ , and  $\chi = 0$ ).

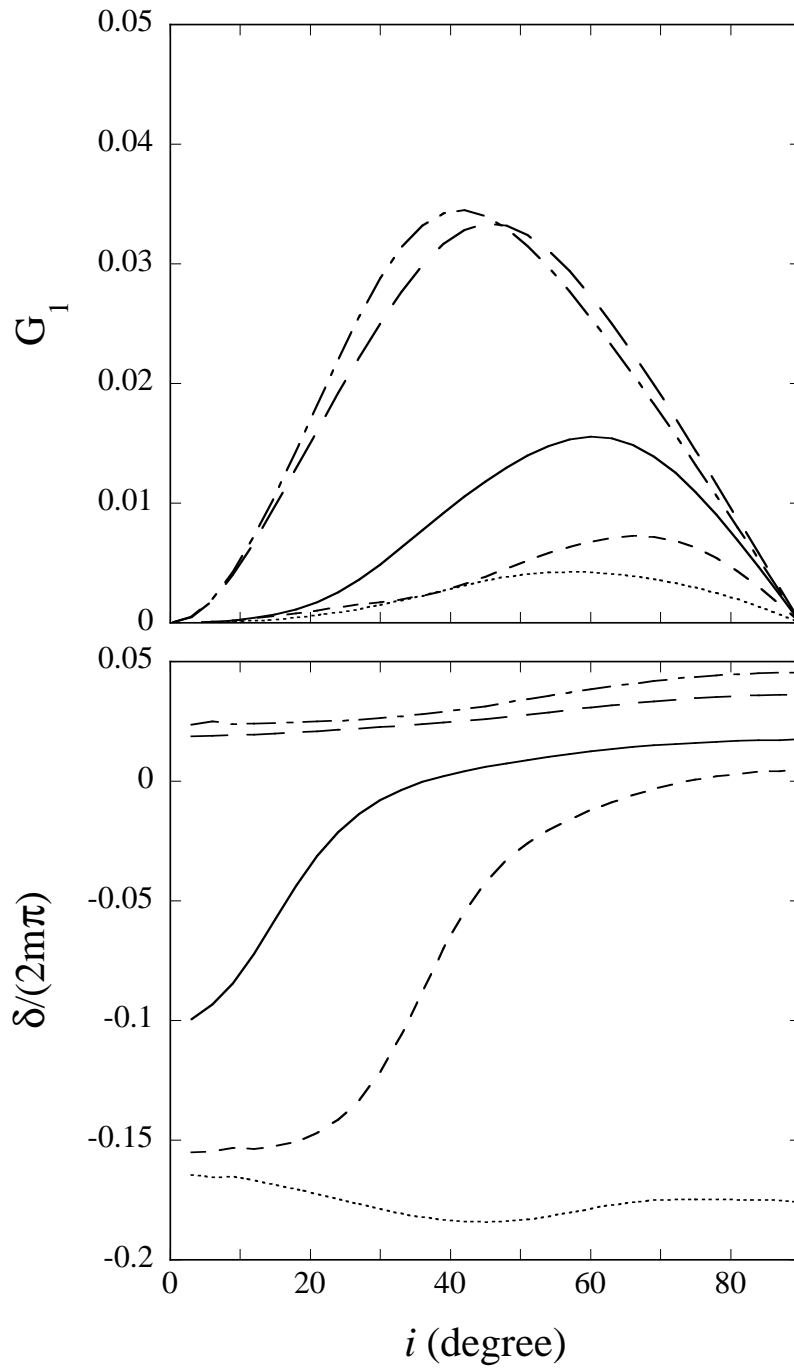


**Figure 6.** Same as Figure 3 but for the fundamental odd  $r$ -mode with  $m = 2$  ( $C_1 = 0$ ,  $C_2 = 0.2$ , and  $\chi = 0$ ).



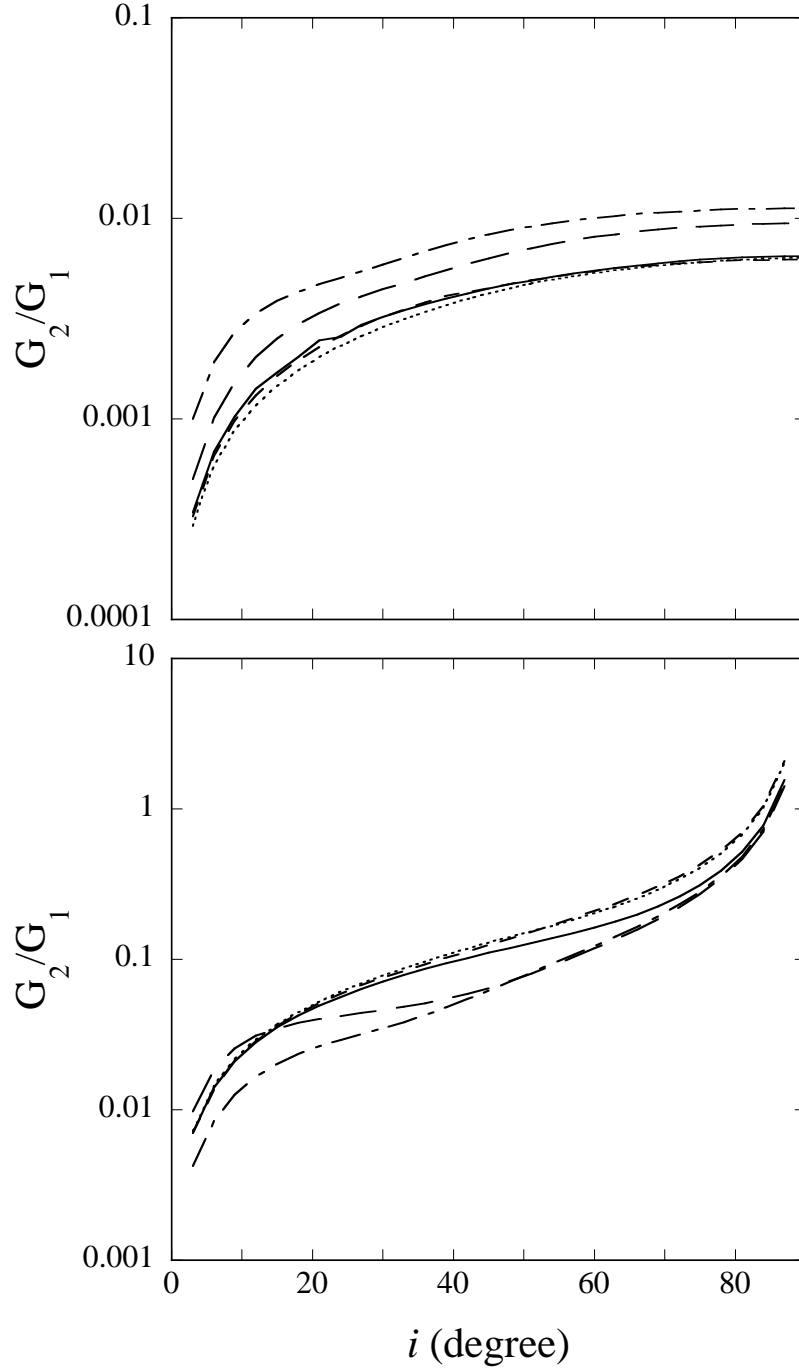


**Figure 7.** Ratio  $G_2/G_1$  as a function of the inclination angle  $i$  for the fundamental even  $r$ -mode with  $m = 1$  (upper panel) and for the fundamental odd  $r$ -mode with  $m = 1$  (lower panel), where  $\bar{\Omega} = 0.2$ , and the various curves represent different radii as in Figure 3. Here, the amplitude normalization for the mode is given by  $|\text{Re}[iT_{l_1}(R)/R]| = 1$  at the surface.

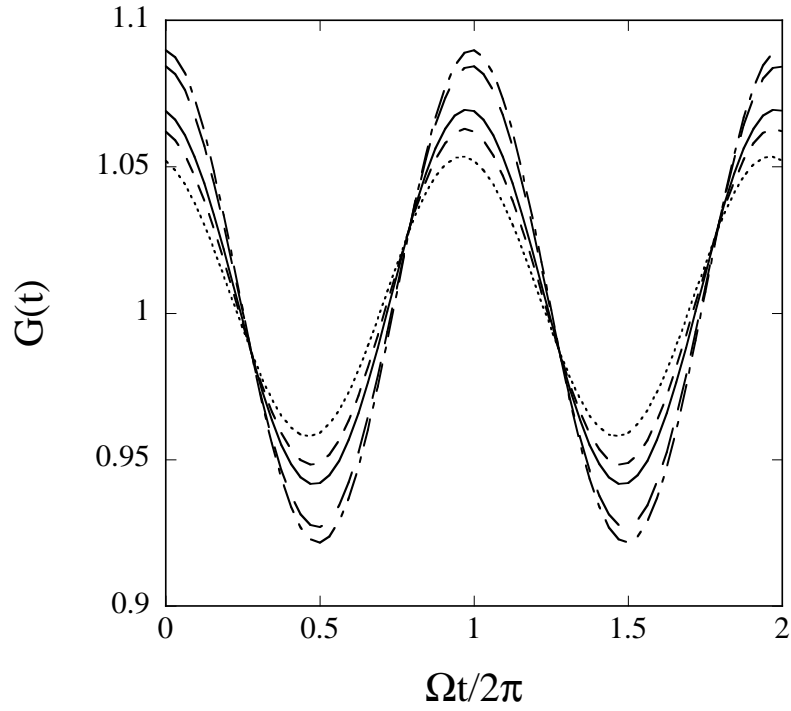


**Figure 8.**  $G(t)$  as a function of  $\Omega t/2\pi$  for the fundamental *even*  $r$ -mode with  $m = 1$  for  $i = 60^\circ$ , where  $C_1 = 0.2$ ,  $C_2 = 0$ ,  $\chi = 0$ , and  $\bar{\Omega} = 0.2$ , and the various curves represent different radii as in Figure 3. Here, the amplitude normalization for the mode is given by  $|\text{Re}[iT_{i_1}(R)/R]| = 1$  at the surface.

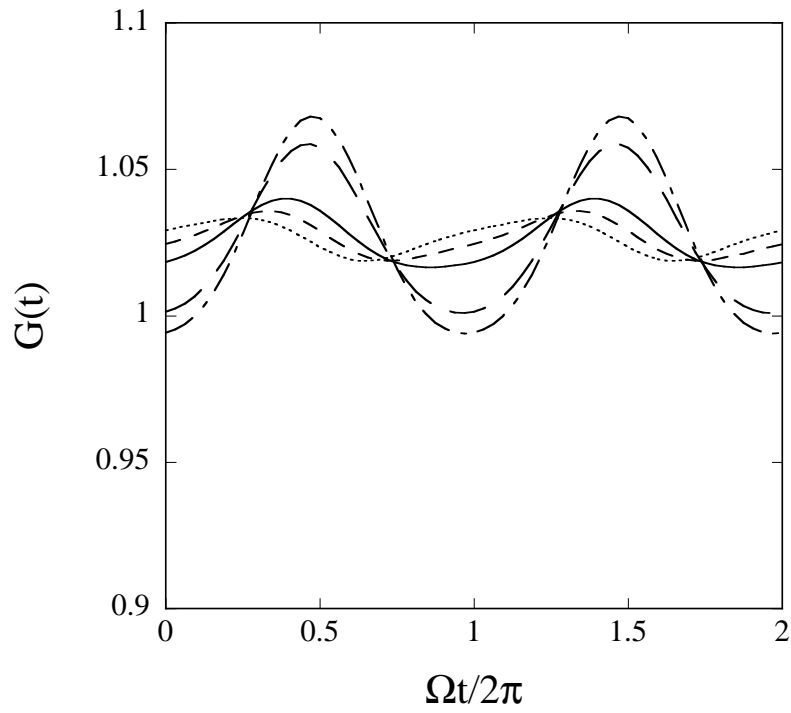


**Figure 9.** Same as Figure 8 but for the fundamental *odd*  $r$ -mode with  $m = 1$ .

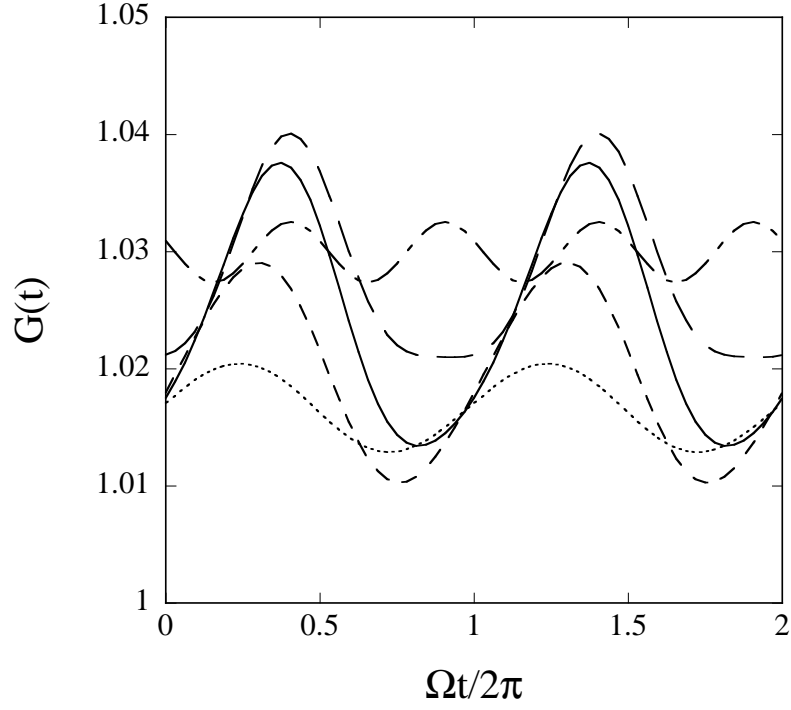


**Figure 10.**  $G(t)$  as a function of  $\Omega t/2\pi$  for the fundamental odd  $r$ -mode with  $m = 1$  for  $R = 10\text{km}$ , where  $C_1 = 0.2$ ,  $C_2 = 0$ ,  $\chi = 0$ , and  $\bar{\Omega} = 0.2$ , and the dotted, short-dashed, solid, long-dashed, and dash-dotted lines indicate the inclination angle  $i = 10^\circ$ ,  $30^\circ$ ,  $50^\circ$ ,  $70^\circ$ , and  $90^\circ$ , respectively. Here, the amplitude normalization for the mode is given by  $|\text{Re}[iT_1(R)/R]| = 1$  at the surface.

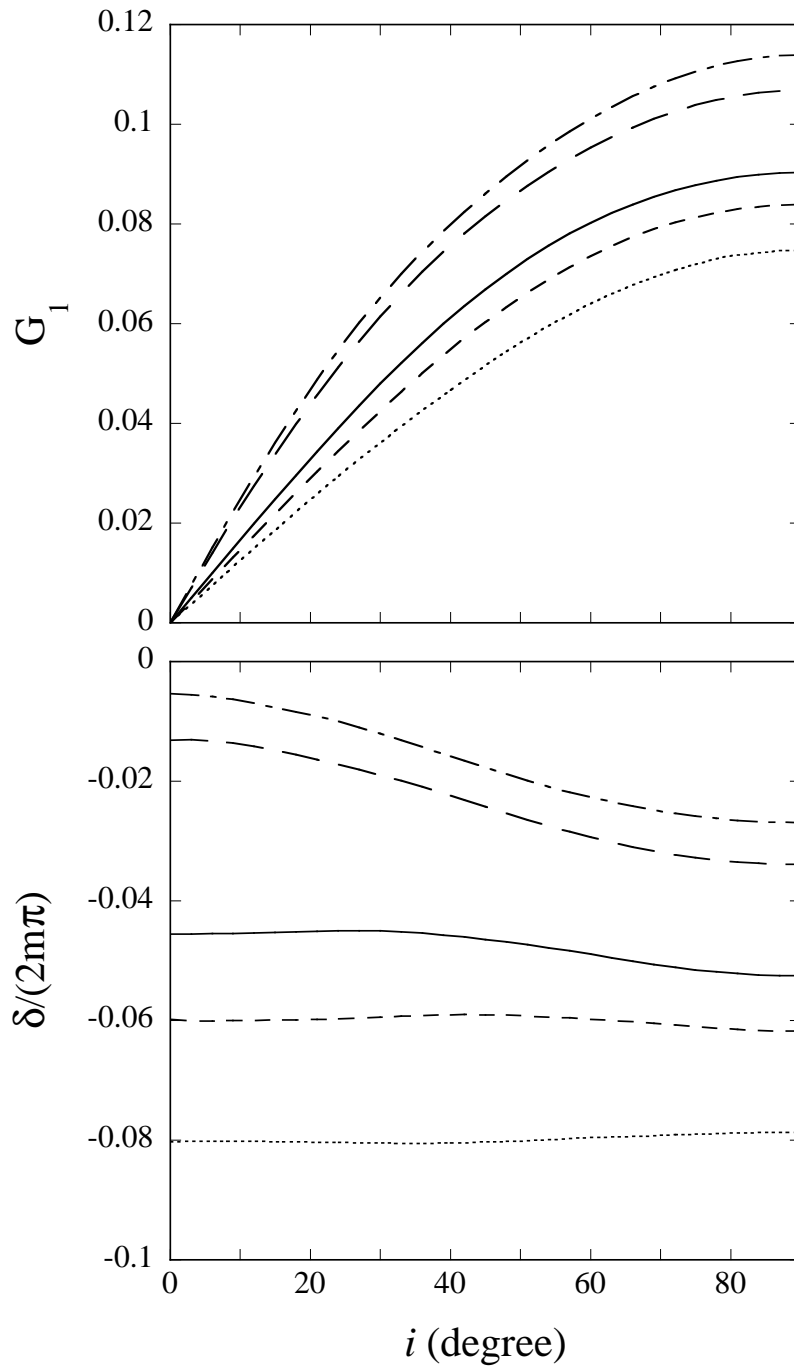


**Figure 11.** Same as Figure 3 but for  $\bar{\Omega} = 0.4$ .

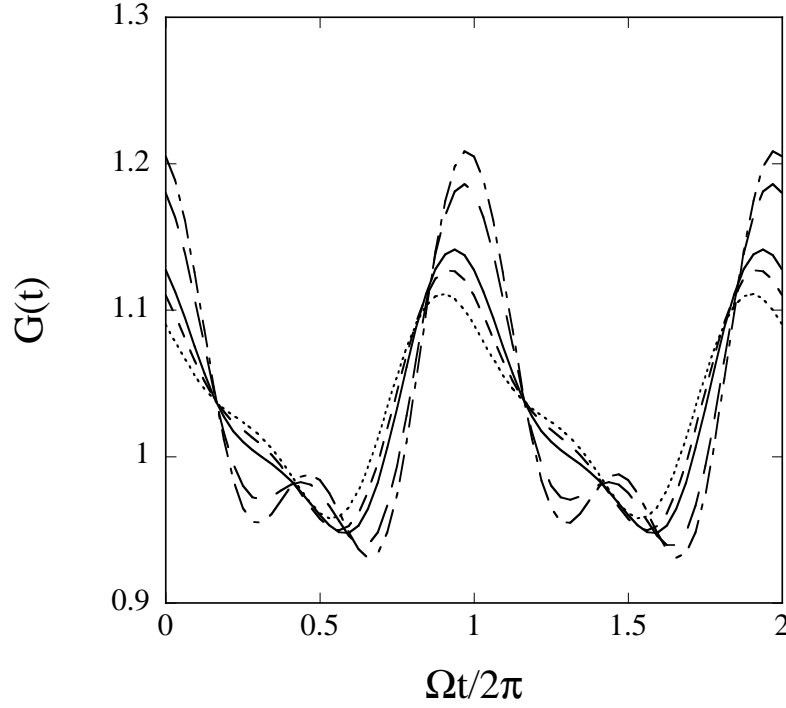


**Figure 12.**  $G(t)$  as a function of  $\Omega t/2\pi$  for the fundamental even  $r$ -modes with  $m = 1$  and  $m = 2$  for  $i = 90^\circ$ , where  $C_1 = C_2 = 0.2$ ,  $\chi = 0$ , and  $\bar{\Omega} = 0.2$ , and the various curves represent different radii as in Figure 3. Here, the amplitude normalization for the mode is given by  $|\text{Re}[iT_{l_1}(R)/R]| = 1$  at the surface.

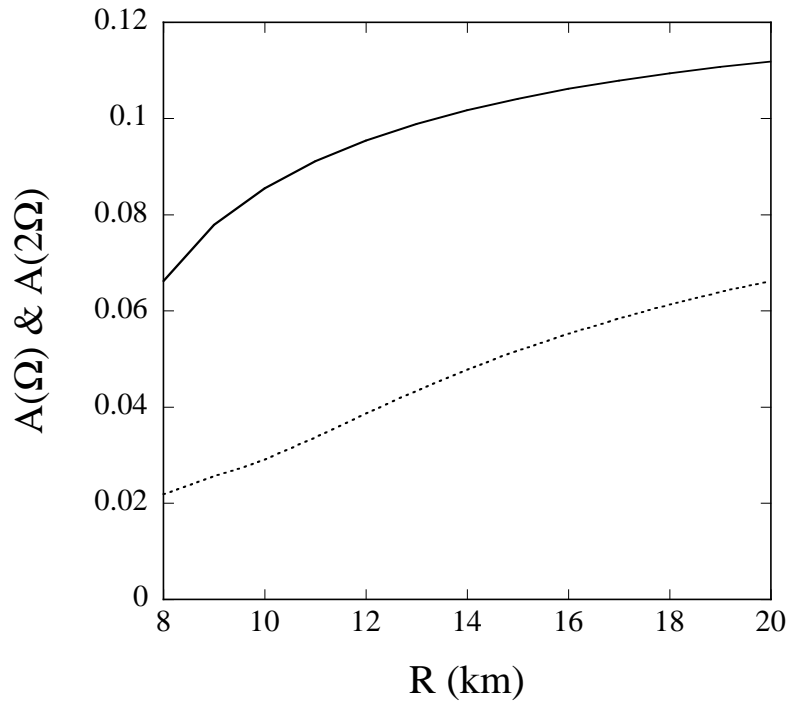


**Figure 13.** Fourier amplitudes  $A(\Omega)$  and  $A(2\Omega)$  as a function of the radius  $R$  for the fundamental even  $r$ -modes with  $m = 1$  and  $m = 2$  for  $i = 90^\circ$ , where  $C_1 = C_2 = 0.2$ ,  $\chi = 0$ , and  $\bar{\Omega} = 0.2$ , and the solid and dotted lines indicate  $A(\Omega)$  and  $A(2\Omega)$ , respectively. Here, the amplitude normalization for the modes is given by  $|\text{Re}[iT_{l_1}(R)/R]| = 1$  at the surface.

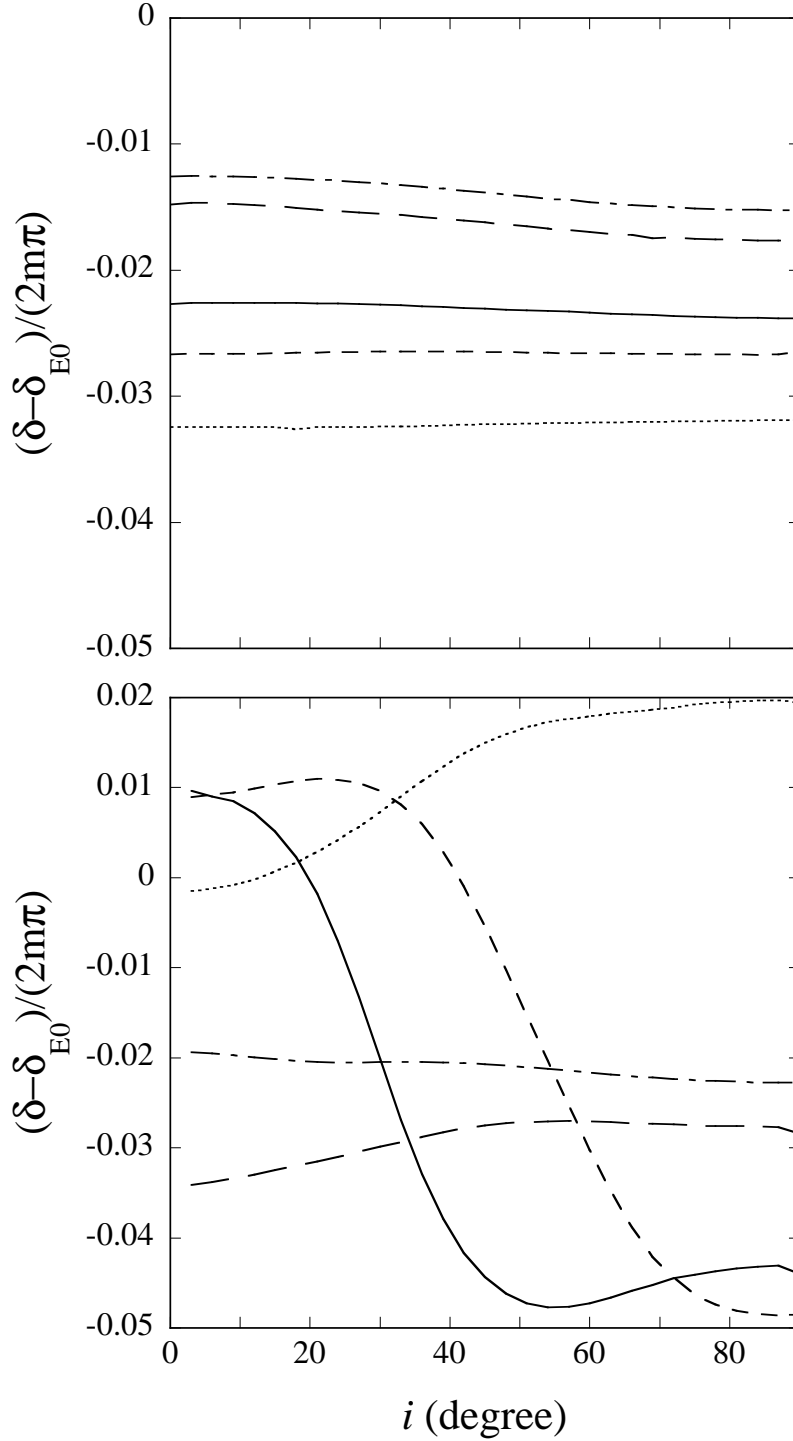


**Figure 14.** Phase shift difference  $(\delta - \delta_{E_0}) / (2m\pi)$  as a function of the inclination angle  $i$  for the fundamental even  $m = 1$   $r$ -mode (upper panel) and for the fundamental odd  $m = 1$   $r$ -mode (lower panel), where  $\bar{\Omega} = 0.2$ ,  $C_1 = 0.2$ ,  $C_2 = 0$ , and  $\chi = 0$ , and the various curves represent different radii as in Figure 3. Here, we have assumed  $k_B T_0 = 2.3 \text{keV}$  and  $E_\infty = E_0 = 1 \text{keV}$  to calculate the function  $G_{E_\infty}(t)$  and the phase shift  $\delta_{E_0}$ . Negative values of  $(\delta - \delta_{E_0}) / (2m\pi)$  indicate hard leads.

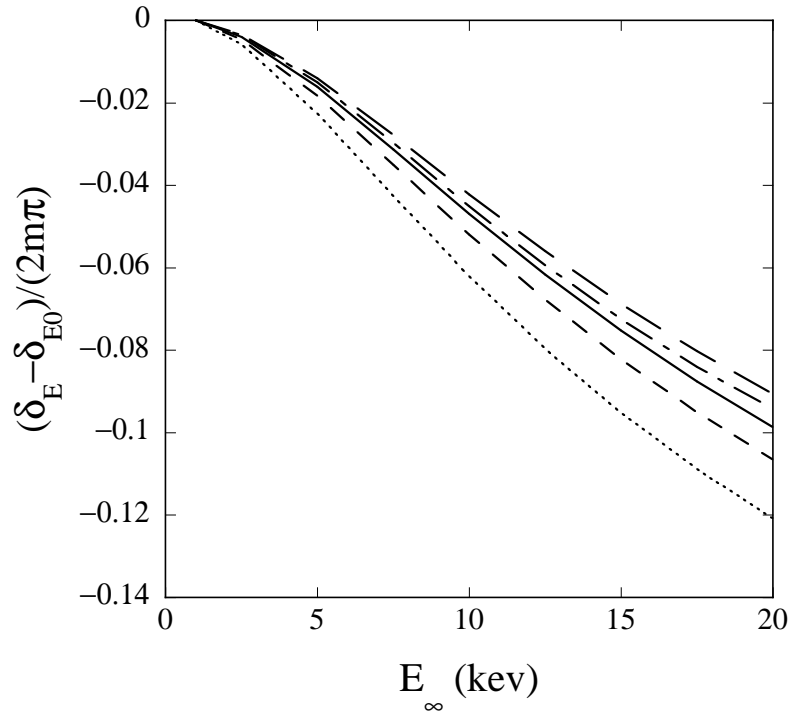


**Figure 15.** Phase shift difference  $(\delta_E - \delta_{E_0})/(2m\pi)$  as a function of the photon energy  $E_\infty = E$  for the fundamental even  $m = 1$   $r$ -mode, where  $\Omega_\infty/2\pi = 400\text{Hz}$ ,  $C_1 = 0.2$ ,  $C_2 = 0$ ,  $\chi = 0$ , and  $i = 60^\circ$ , and the various curves represent different radii as in Figure 3. Here, we have assumed  $k_B T_0 = 2.3\text{keV}$  and  $E_\infty = E_0 = 1\text{keV}$  to calculate the function  $G_{E_\infty}(t)$  and the phase shift difference  $(\delta_E - \delta_{E_0})/(2m\pi)$ , the negative values of which indicate hard leads.

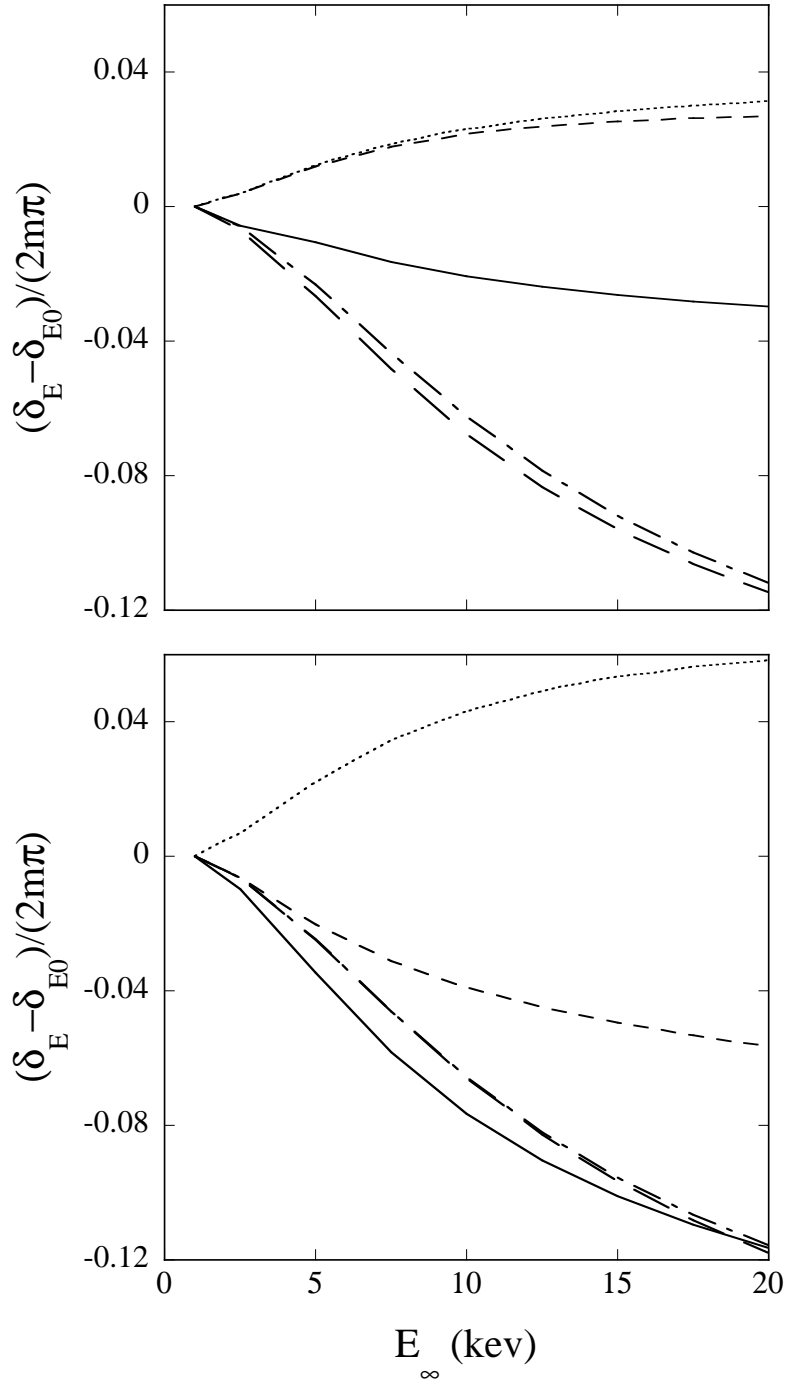


**Figure 16.** Phase shift difference  $(\delta_E - \delta_{E_0})/(2m\pi)$  as a function of the photon energy  $E_\infty = E$  for the fundamental odd  $m = 1$   $r$ -mode for  $i = 30^\circ$  (upper panel) and for  $i = 60^\circ$  (lower panel), where  $\Omega_\infty/2\pi = 400\text{Hz}$ ,  $C_1 = 0.2$ ,  $C_2 = 0$ , and  $\chi = 0$ , and the various curves represent different radii as in Figure 3. Here, we have assumed  $k_B T_0 = 2.3\text{keV}$  and  $E_\infty = E_0 = 1\text{keV}$  to calculate the function  $G_{E_\infty}(t)$  and the phase shift difference  $(\delta_E - \delta_{E_0})/(2m\pi)$ , the negative values of which indicate hard leads.